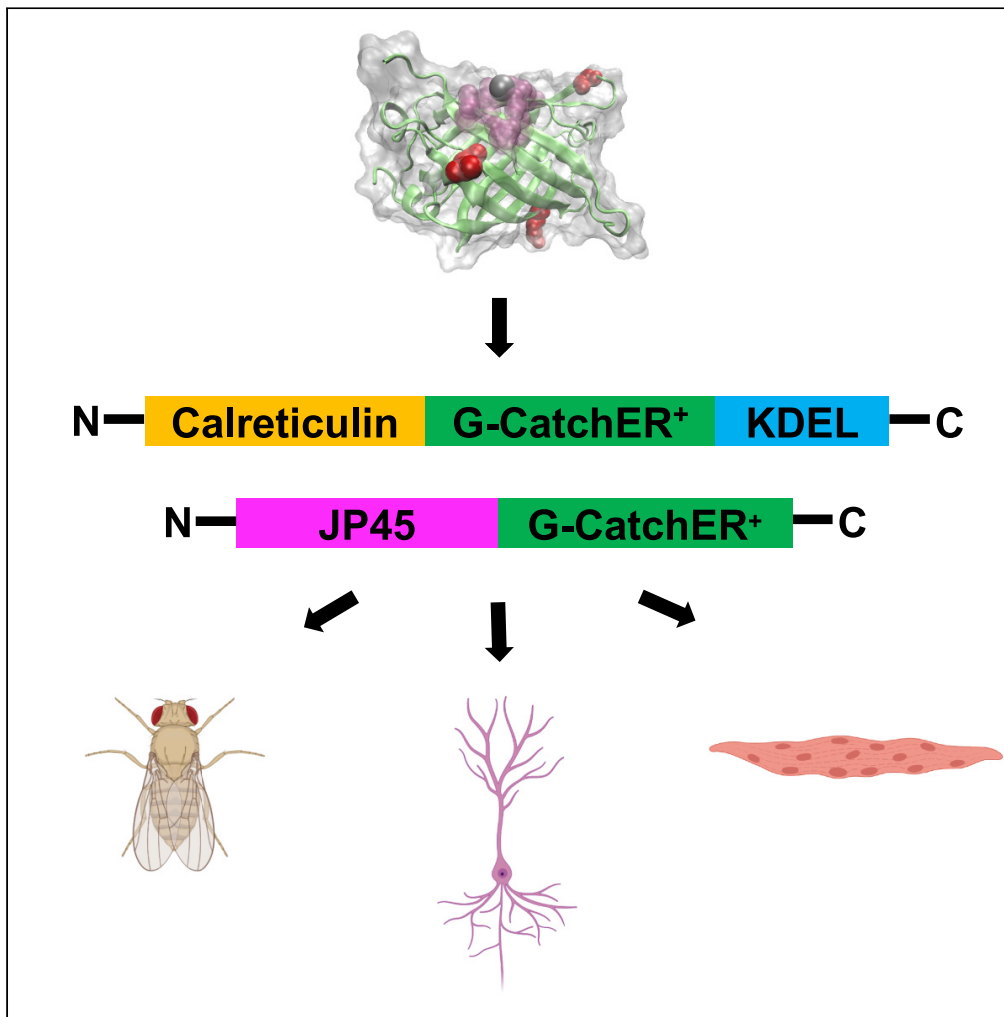**Article**

Rapid subcellular calcium responses and dynamics by calcium sensor G-CatchER+

Florence N.
Reddish,
Cassandra L.
Miller, Xiaonan
Deng, ..., Susan
Treves, Francesco
Zorzato, Jenny J.
Yang

jenny@gsu.edu

HIGHLIGHTS

G-CatchER+ exhibits superior kinetics with 1:1 stoichiometry than G-CEPIA1er

G-CatchER+ captures spatially confined ER Ca^{2+} dynamics in hippocampal neurons

G-CatchER+-JP45 reports rapid Ca^{2+} signals adjacent to the junctional SR membrane

G-CatchER+ reports stimulus-evoked SR local Ca^{2+} dynamics in *Drosophila* muscle

iScience

Article

Rapid subcellular calcium responses and dynamics by calcium sensor G-CatchER$^+$

Florence N. Reddish,[1,8] Cassandra L. Miller,[1,8] Xiaonan Deng,[1,8] Bin Dong,[1] Atit A. Patel,[2,3] Mohammad A. Ghane,[2,3] Barbara Mosca,[4] Cheyenne McBean,[1] Shengnan Wu,[5] Kyril M. Solntsev,[6] You Zhuo,[1] Giovanni Gadda,[1] Ning Fang,[1] Daniel N. Cox,[2,3] Angela M. Mabb,[2,3] Susan Treves,[4,7] Francesco Zorzato,[4,7] and Jenny J. Yang[1,9,*]

SUMMARY

The precise spatiotemporal characteristics of subcellular calcium (Ca^{2+}) transients are critical for the physiological processes. Here we report a green Ca^{2+} sensor called "G-CatchER$^+$" using a protein design to report rapid local ER Ca^{2+} dynamics with significantly improved folding properties. G-CatchER$^+$ exhibits a superior Ca^{2+} on rate to G-CEPIA1er and has a Ca^{2+}-induced fluorescence lifetimes increase. G-CatchER$^+$ also reports agonist/antagonist triggered Ca^{2+} dynamics in several cell types including primary neurons that are orchestrated by IP$_3$Rs, RyRs, and SERCAs with an ability to differentiate expression. Upon localization to the lumen of the RyR channel (G-CatchER$^+$-JP45), we report a rapid local Ca^{2+} release that is likely due to calsequestrin. Transgenic expression of G-CatchER$^+$ in *Drosophila* muscle demonstrates its utility as an *in vivo* reporter of stimulus-evoked SR local Ca^{2+} dynamics. G-CatchER$^+$ will be an invaluable tool to examine local ER/SR Ca^{2+} dynamics and facilitate drug development associated with ER dysfunction.

INTRODUCTION

Calcium (Ca^{2+}) is a major modulator of a multitude of cellular, biological, and pathological processes in organisms (Clapham, 2007) that is achieved using a Ca^{2+} signaling toolkit consisting of Ca^{2+} pumps, Ca^{2+} channels, receptors, and Ca^{2+} binding proteins (CaBPs) such as calsequestrin, calreticulin, parvalbumin, calmodulin etc. (Figure 1C). As the primary intracellular Ca^{2+} store, the endoplasmic reticulum (ER) or the sarcoplasmic reticulum (SR) found in muscle cells is central to Ca^{2+} signaling by modulating Ca^{2+} transients with differential timescales that govern key biological functions (Berridge et al., 2003). The task of converting extracellular stimuli into a coded intracellular Ca^{2+} signal, wave, or oscillation lies within the ER/SR in combination with a non-uniform distribution of CaBPs. These modulators of the Ca^{2+} signal create spatially diverse nanocompartments with differential Ca^{2+} concentrations within the ER/SR lumen via their spatial distribution and response dynamics (Papp et al., 2003). The morphology of the ER, especially in neural cells, is highly heterogeneous with strong plasticity tailored to various chemical and dynamic tasks in different areas of the cell, as well as between different cell types (Bourne and Harris, 2012). On the other hand, in skeletal muscle the RyR1 of the SR has a specialized arrangement in order to ensure a quick delivery of the Ca^{2+} needed for muscle contraction in response to membrane depolarization (Petersen et al., 2001; Berridge, 2002). The hypothesis that differential subcellular dynamics play an essential role in the regulation of rapid biological and pathological processes has not been fully addressed due to lack of fast Ca^{2+} sensors.

Early efforts investigating ER Ca^{2+} release involved Ca^{2+} dyes to monitor Ca^{2+} transients indirectly with antipyrylazo III (Schneider et al., 1987; Melzer et al., 1987) and directly with fluo-5N (Kabbara and Allen, 2001). Genetically encoded Ca^{2+} indicators (GECIs) based on calmodulin (CaM) (Miyawaki et al., 1997) such as G-CEPIA1er (Suzuki et al., 2014a) and FRET pairs have been very informative but have limitations that include non-specific distribution within intracellular organelles, narrow Ca^{2+} affinities that are close to the intracellular environment, non-linearity due to multiple Ca^{2+} binding sites, and slow Ca^{2+} kinetics
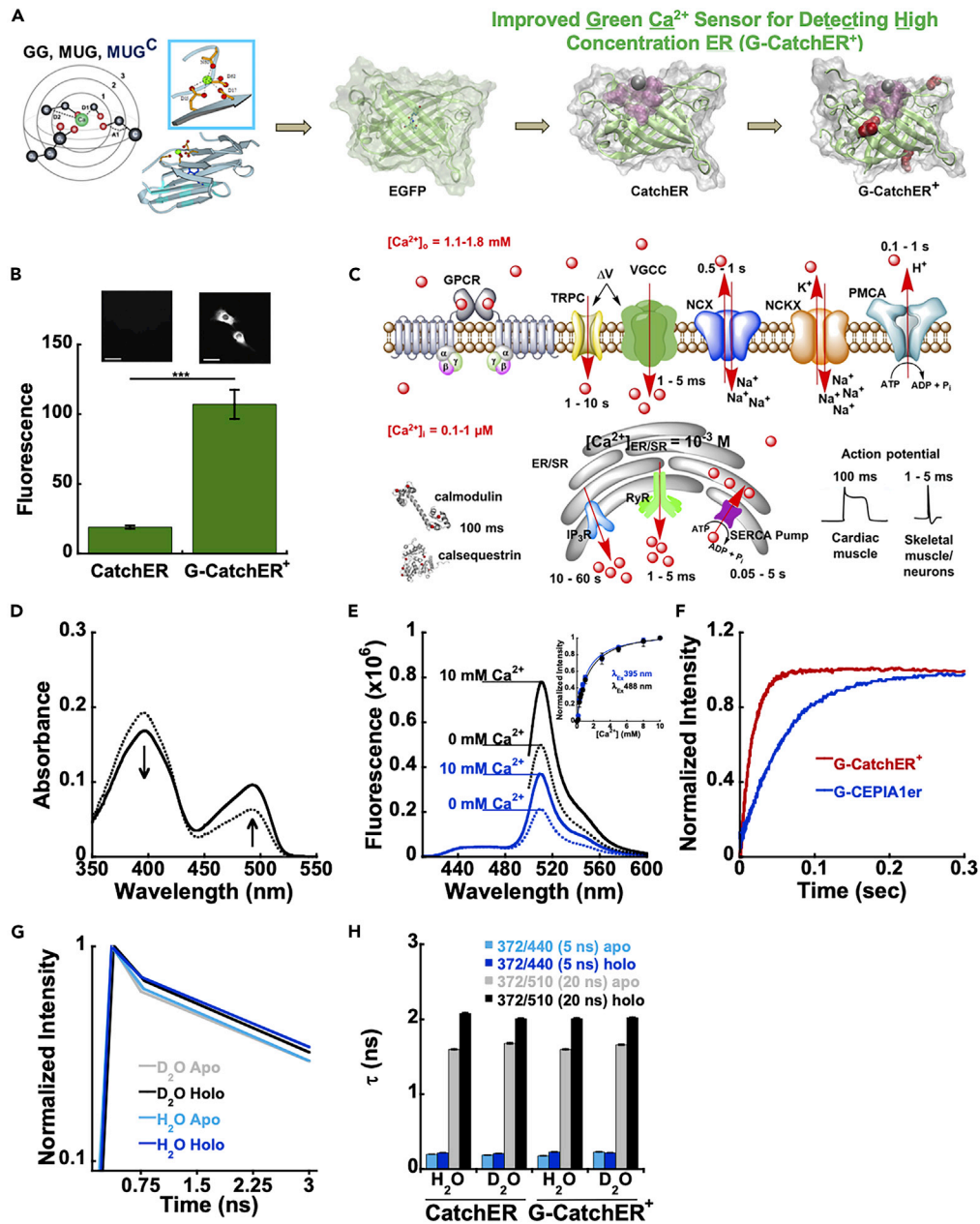
Figure 1. Design and *in vitro* properties of G-CatchER⁺

(A) Design of Ca^{2+} binding sites using MUG (MUltiple Geometries) algorithm. EGFP was modified with a direct Ca^{2+} binding site. Both CatchER and G-CatchER⁺ were designed using these techniques (binding site residues are highlighted in pink, residues mutated from CatchER to G-CatchER⁺ are highlighted in red, and Ca^{2+} is represented with the silver ball).

(B) Mutations S175G, S30R, and Y39N were added to CatchER to improve its brightness and thermostability at 37°C. G-CatchER⁺ contains all three mutations. n = 10 for CatchER and G-CatchER⁺. Statistical significance was determined using unpaired student t test. p < 0.0001.

(C) Components of the Ca^{2+} signaling toolkit help shape the spatial-temporal signal. Calcium signaling is mediated by various pumps, channels, receptors, and CaBPs to control intracellular Ca^{2+} release from calcium storage organelles such as the ER/SR. The rapid action of Ca^{2+} release receptors and pumps lining the ER/SR membrane along with the fast conformational changes of some CaBPs rapidly convert the signal for action potential generation in muscle contraction and neuron activation.

(D) Absorbance spectra of 10 μM G-CatchER⁺ sample before titration with 10 μM EGTA (dashed line) and after titrating up to 10 mM Ca^{2+} (solid line). Arrows indicate the increase and decrease in the 488 nm and 395 nm excitation peaks with the addition of Ca^{2+}.

Figure 1. *Continued*

(E) Fluorescence increase of G-CatchER$^+$ in response to addition of Ca^{2+} excited at 395 nm (blue) and 488 nm (black), respectively, with emission monitored at 510 nm. Slit widths for excitation and emission were 0.25 mm. *Inset,* Binding curves were fit with a 1:1 binding equation to obtain the K$_d$.

(F) Comparison of Ca^{2+}-associated kinetics of G-CatchER$^+$ and G-CEPIA1er.

(G) Fluorescence decay curves of G-CatchER$^+$ in both D$_2$O and H$_2$O when excited at 372 nm, with and without Ca^{2+}.(H) Average lifetimes of G-CatchER$^+$ in both D$_2$O and H$_2$O when excited at 372 nm, with and without Ca^{2+}. Scale bars, 20 μm. See also Figures S1 and S2 and Tables S1–S3.

(Sztretye et al., 2011a; Landolfi et al., 1998; Jimenez-Moreno et al., 2010). Thus, there is a pressing need to design Ca^{2+} sensors having the capacity to quantify these differential subcellular Ca^{2+} dynamics in both biological and pathological states (Tang et al., 2015, 2020). To fill in this gap, we initially developed a genetically encoded green Ca^{2+} sensor, CatchER, by creating a single Ca^{2+} binding site directly onto the enhanced green florescent protein (EGFP) scaffold (Tang et al., 2011).

Here we report the development of an improved version of CatchER, G-CatchER$^+$, with optimized folding at physiological temperature. G-CatchER$^+$ specifically reports rapid global ER/SR Ca^{2+} dynamics in various cell types including neuron and muscle cells. G-CatchER$^+$ exhibits a significantly faster Ca^{2+} on rate than G-CEPIA1er with enhanced Ca^{2+}-dependent fluorescence increases as a result of increased fluorescence lifetime upon Ca^{2+} binding. In addition, G-CatchER$^+$ has the capacity to monitor rapid local ER/SR Ca^{2+} changes in multiple cell types and in a subcellular environment in both neuron and excitation-contraction (EC) coupling processes.

RESULTS

Generation and optimization of G-CatchER$^+$

G-CatchER$^+$ was designed by creating a single Ca^{2+} binding site with negatively charged residues directly onto EGFP like CatchER (Figure 1A)(Tang et al., 2011). To overcome folding limitations and to increase dynamic range of CatchER for mammalian cell applications, we introduced mutations S30R, Y39N, and S175G individually and in combination to create G-CatchER$^+$ (Pedelacq et al., 2006; Siemering et al., 1996). G-CatchER$^+$ exhibits significantly improved folding stability and subsequent fluorescence. These engineered proteins were expressed in *Escherichia coli* and purified using established methods (Figure S1). G-CatchER$^+$ is among several variants that exhibited an improvement in their inherent optical properties compared with CatchER when investigated using spectroscopic methods (Table S2 and Figure S1). G-CatchER$^+$ is also among several variants that exhibits less pH sensitivity with Ca^{2+} as determined by pK$_a$ values of 7.37 $\pm$ 0.01 and 6.80 $\pm$ 0.01 with and without Ca^{2+}, respectively (Table S3 and Figure S2). C2C12 myoblast cells expressing G-CatchER$^+$ experienced a 5-fold increase in intensity (107.2 $\pm$ 3.3) compared with CatchER (19.1 $\pm$ 0.3) at 37°C using epifluorescence microscopy (Figure 1B). Each individual mutation had minimal effects on the intensity at 37°C compared with the combination of all three (Figure S1).

Metal binding affinity of G-CatchER$^+$ *in vitro* and in cells

The Ca^{2+} binding affinity of G-CatchER$^+$ was determined using fluorescence spectroscopy and epifluorescence microscopy. Saturation with Ca^{2+} resulted in a concurrent absorbance increase at 488 nm and decrease at 395 nm for G-CatchER$^+$ (Figure 1D) and variants (Figure S1). G-CatchER$^+$ had gradual incremental increases (~ 60%) in fluorescence intensity with a maximum peak at 510 nm upon addition of Ca^{2+} when excited at both 395 nm and 488 nm. Such fluorescence excitation changes at 395 nm and 488 nm were well fitted to a 1:1 binding equation with a determined K$_d$ value for Ca^{2+} binding of 1.2 $\pm$ 0.2 mM (Figure 1E and Table S1). The average Ca^{2+} K$_d$ in the presence of 150 mM KCl and *in situ* in Cos-7 and HEK293 cells in the presence of physiological concentrations of Mg^{2+}, Na$^+$, K$^+$, and small molecules in the ER/SR were decreased, suggesting the role of an electrostatic interaction for Ca^{2+} binding (Figure S2).

Measuring the rapid kinetic properties of G-CatchER$^+$

We next used stopped-flow spectrofluorometry to determine the time courses for Ca^{2+} association to and dissociation from G-CatchER$^+$. Irrespective of the Ca^{2+} concentration between 0.1 mM and 5.0 mM, the fluorescence of G-CatchER$^+$ increased with a k$_{obs}$ value of 62 s^{-1} (Figure S2), consistent with a conformational change of a Ca^{2+}-G-CatchER$^+$ complex being rate limiting for the overall process. When Ca^{2+}-loaded

G-CatchER$^+$ was mixed with 2.0 mM EGTA, the fluorescence decreased with a k_{obs} value of 63 s^{-1}, indicating rapid release of Ca^{2+} from the Ca^{2+}-G-CatchER$^+$ complex (Figure S2). For comparison, when G-CEPIA1er was used instead of G-CatchER$^+$, the k_{obs} value for Ca^{2+} release from the complex was similar (k_{obs} = 81 s^{-1} versus 63 s^{-1}), but the k_{obs} value for fluorescence increase associated with Ca^{2+} binding was four times slower (k_{obs} = 15 s^{-1} versus 62 s^{-1}) (Figures 1F and S2).

Calcium binding increases G-CatchER$^+$'s lifetime leading to enhanced fluorescence

We next applied time-resolved optical methods and hydrogen/deuterium isotope exchange to understand the origin of Ca^{2+}-induced optical property changes of G-CatchER$^+$. Fluorescence decay curves of R*OH and R*O$^-$ were measured at pH 7.4 (Figure S2). The decay of R*OH and the directly excited R*O$^-$ form (at 467 nm) could be fitted to a double-exponential that gave rise to average lifetimes of 0.19 ns and 2.61 ns, respectively (Figures 1G and 1H). Upon Ca^{2+} binding, there was a 30% mean fluorescence lifetime increase of the indirectly excited anionic chromophore. For the indirectly excited (at 372 nm) R*O$^-$ form, a fast quenching component within the first 2 ns was detected, which was followed by a long asymptotic decay closely approaching the lifetime of the directly excited R*O$^-$. Further lifetime studies in D$_2$O confirmed that such a lifetime increase of G-CatchER$^+$ is a result of delayed proton geminate recombination and is caused by a combination of acid-base equilibrium and arrangement differences of the proton network with the chromophore between Ca^{2+} free and the Ca^{2+} binding form (Zhuo et al., 2015). Ca^{2+} also exhibited a strong inhibition of the excited state proton transfer nonadiabatic geminate recombination in protic (versus deuteric) medium (Figure S2). Such a Ca^{2+}-dependent lifetime change explains the Ca^{2+}-dependent fluorescence increase and indicates a potential future application of G-CatchER$^+$ for lifetime imaging.

Quantitative measurements of drug-induced ER/SR calcium changes in multiple cell types

G-CatchER$^+$ was highly enriched in the ER/SR of C2C12 myoblasts (Figure 2A) as demonstrated by labeling of C2C12 cells expressing G-CatchER$^+$ with the ER-specific marker, ER-Tracker red, yielding a Pearson's co-efficient of 0.91 (Figure 2A). G-CatchER$^+$ could also quantitatively monitor drug-induced [Ca^{2+}]$_{ER}$ changes in multiple cell types using highly inclined thin illumination (HILO) (Tokunaga et al., 2008) (Figures 2B–2D) and epifluorescence microscopy (Figure S3). Although CatchER$^+$ is likely to have a differential expression in different cells, fluorescence response (changes) in C2C12 cells upon the addition of the RyR agonist in different cells can be accurately determined with normalization (Figure 2E). After normalizing the fluorescence change by dividing the baseline fluorescence before treatment, all cells (n = 32) have a similar degree of release responses (−0.46 ± 0.01) (Figures 2E–2G and Table 1).

G-CatchER$^+$ responses to multiple ER-Ca^{2+} modulators were assessed using HILO and epifluorescence. C2C12 cells, which express high levels of RyRs, had the strongest peak (−0.46 ± 0.01) following addition of 1 mM 4-cmc (Figure 2B and Table 1). On the other hand, Cos-7 and HEK293 cells had a smaller release following addition of 0.5 mM 4-cmc (−0.12 ± 0.01 and −0.22 ± 0.02, respectively) because higher concentrations of 4-cmc negatively affected these cell types (Table 1). In addition, HeLa cells treated with 1 mM 4-cmc still had a markedly lower response (−0.24 ± 0.01) (Table 1). Intriguingly, 0.5 mM ATP treatment to activate P$_2$YR and subsequent ER Ca^{2+} release via the IP$_3$ receptor in all three cell types (C2C12, Cos-7, and HEK293 cells) resulted in a smaller amplitude change than 4-cmc but was in a similar range to each other (Figure 2D and Table 1). We also observed similar changes (−0.13 ± 0.01) in HeLa cells following treatment of histamine, which activates the histamine receptor (H1R) to trigger PLC-mediated ER Ca^{2+} release (Table 1). Similarly, 50 µM treatment of the SERCA pump inhibitor CPA, which prevents the refilling of ER Ca^{2+} stores until washout, led to a reduction in ER Ca^{2+} levels in these three cell types with more variable amplitude peak responses in comparison to ATP (Table 1). The vehicle control for CPA, DMSO, showed a subtle yet insignificant effect in C2C12 cells (Figure S3J). We observed consistent ER Ca^{2+} release using epifluorescence microscopy and further monitored changes in other compounds, thapsigargin and caffeine, that cause extrusion of Ca^{2+} from the ER using G-CatchER$^+$ (Figure S3 and Table 1).

G-CatchER$^+$ captures spatially confined ER calcium dynamics in neurons

We next determined if G-CatchER$^+$ could report accurate changes in ER Ca^{2+} levels in neurons, which have elaborate and complex ER morphologies (Terasaki et al., 1994; Spacek and Harris, 1997). G-CatchER$^+$ was expressed in primary hippocampal neurons with no overt effects on overall health (Figure S4). Similar to immortalized cells, G-CatchER$^+$ highly colocalized with ER markers (data not shown). With the addition of 0.5 mM 4-cmc, we identified a significant difference in the G-CatchER$^+$ response between secondary branchpoints and secondary dendrites (Figures 3A and 3B). Treatment with 50 µM CPA resulted in a smaller
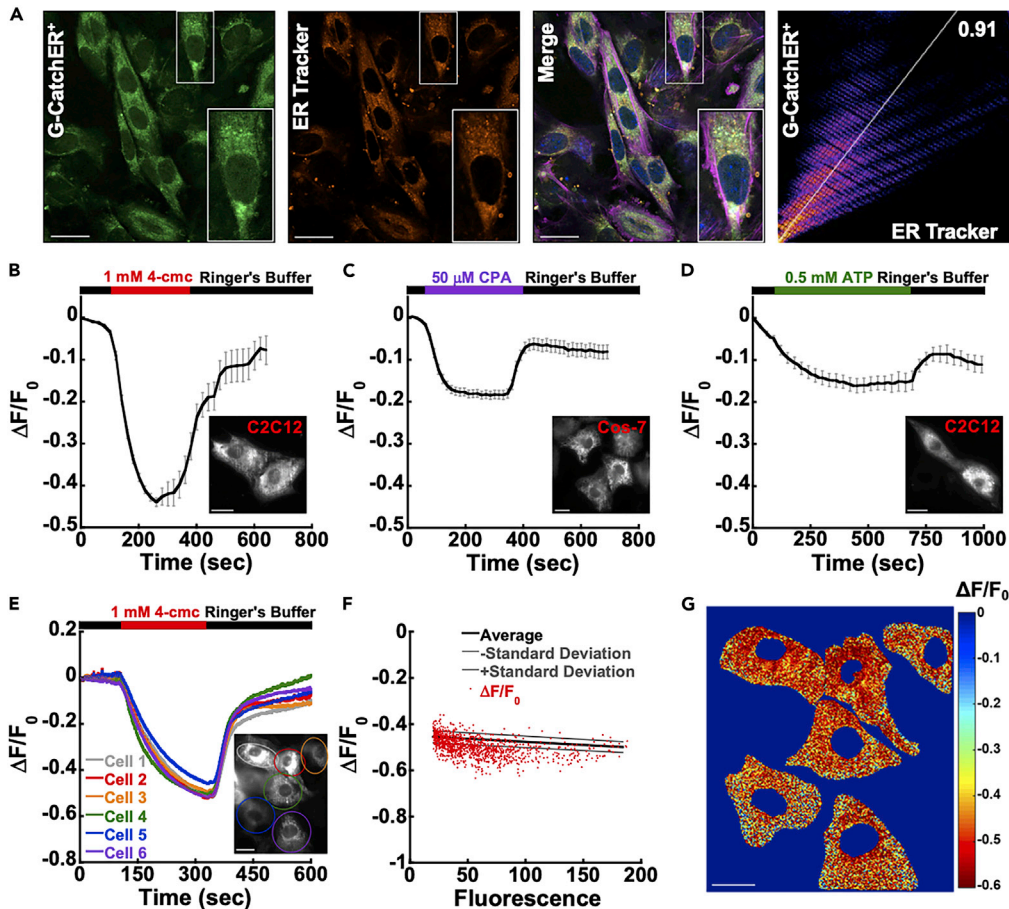
Figure 2. G-CatchER+ ER localization and HILO imaging leads to quantitative measurement of calcium responses

(A) G-CatchER+ expression at 488 nm (green), ER-Tracker red staining at 555 nm (orange), DAPI staining for the nucleus at 405 nm (blue), actin staining with phalloidin at 633 nm for structure (magenta). Insets are zoomed in regions of one cell from the outlined white box. G-CatchER+ expression has a Pearson's coefficient of 0.91 when compared with ER-Tracker red.

(B) 1 mM of 4-cmc was added to initiate a release of Ca^{2+} from the ER in C2C12 cells. n = 21 cells. F_0 is the fluorescence intensity at the initial time point of measurement and $\Delta F = F_t - F_0$, where F_t is the fluorescence intensity at time t.

(C) 50 μM of CPA was added to initiate a release of Ca^{2+} from the ER in Cos-7 cells. n = 30 cells.

(D) 500 μM of ATP was added to initiate a release of Ca^{2+} from the ER in C2C12 cells. n = 9 cells.

(E) C2C12 cells plotted as normalized $\Delta F/F_0$ in response to 1 mM 4-cmc showing overall release of whole cells is similar where each color circle matches each cell in inset.

(F) Pixel by pixel plot of $\Delta F/F_0$ response from the six cells with R = 0.42.

(G) $\Delta F/F_0$ intensity map of the six cells analyzed in E&F. Scale bars, 20 μm.

See also Figure S3.

change in amplitude with no significant differences between different neuronal regions (Figures 3C and 3D). Subcellular effects with refilling were also less apparent with CPA, which was in part contributed by a DMSO effect (Figures 3C and 3D). We determined the maximum fluorescence of G-CatchER+ in different regions of neurons by applying 50 μM of ionomycin and 10 mM Ca^{2+} ($\Delta F/F$; soma: 0.58 ± 0.13; primary dendrites: 0.35 ± 0.05; primary branchpoints: 0.56 ± 0.13; secondary dendrites: 0.21 ± 0.04; secondary branchpoints: 0.42 ± 0.10; p = 0.06) (Figure S4). Basal $[Ca^{2+}]_{ER}$ in different neuronal regions was calculated using established methods (soma: 167.8 ± 45.5 μM; primary dendrites: 308.2 ± 56.9 μM; primary branchpoints: 192.3 ± 45.7 μM; secondary dendrites: 458.8 ± 88.5 μM; secondary branchpoints: 253.0 ± 42.9 μM) (Figure S4E) (de Juan-Sanz et al., 2017). We found that the estimated ER Ca^{2+} concentration in secondary dendrites was significantly higher than the soma and primary branchpoints (p = 0.02), indicating that ER Ca^{2+} concentrations vary in hippocampal neuronal regions.

Table 1. Epifluorescence and HILO imaging responses of G-CatchER$^+$ to multiple reagents and cell types

Cell Type	Drug Type	Epifluorescence Imaging				HILO Imaging			
		[Drug] (µM)	$\Delta F/F_0$	Cell #	Trial #	[Drug] (µM)	$\Delta F/F_0$	Cell #	Trial #
C2C12	4-cmc	200	-0.19 ± 0.01	43	9	1000	-0.46 ± 0.01	32	11
Cos-7	4-cmc	200	-0.15 ± 0.08	24	6	500	-0.12 ± 0.01	36	7
HEK293	4-cmc	200	-0.24 ± 0.07	27	5	500	-0.22 ± 0.02	40	6
HeLa	4-cmc	ND	ND	ND	ND	1000	-0.24 ± 0.01	10	2
Hip. Neurons	4-cmc	ND	ND	ND	ND	500	-0.38 ± 0.04	9	3
C2C12	CPA	15	-0.24 ± 0.02	35	5	50	-0.26 ± 0.02	18	7
Cos-7	CPA	15	-0.26 ± 0.02	10	3	50	-0.17 ± 0.01	31	6
HEK293	CPA	15	-0.23 ± 0.01	32	5	50	-0.23 ± 0.01	18	3
Hip. Neurons	CPA	ND	ND	ND	ND	50	-0.10 ± 0.04	8	3
C2C12	ATP	100	-0.10 ± 0.03	26	8	500	-0.14 ± 0.01	12	7
Cos-7	ATP	100	-0.15 ± 0.02	24	9	500	-0.12 ± 0.02	13	3
HEK293	ATP	100	-0.10 ± 0.02	19	4	500	-0.16 ± 0.01	24	3
HeLa	Histamine	ND	ND	ND	ND	100	-0.13 ± 0.01	33	9
Hip. Neurons	DHPG	ND	ND	ND	ND	100	-0.07 ± 0.01	8	8

Data represent mean $\pm$ SEM error. ND, no data; $\Delta F/F_0$, change in fluorescence signal over initial fluorescence in response to drugs. Data collected at room temperature; Hip. Neurons, primary hippocampal neurons that have been cultured for 13 days *in vitro*. See also Figures S3 and S7.

The concerted actions of spatially confined Ca^{2+} flux provide the appropriate threshold response for various forms of synaptic plasticity (Citri and Malenka, 2008). Long-term depression (LTD) via activation of group I metabotropic glutamate receptors (mGluR-LTD) is a type of synaptic plasticity that results in IP$_3$-mediated release of ER Ca^{2+} stores and is associated with an increase in the removal of Ca^{2+} permeable α-amino-3-hydroxy-5-methyl-4-isoxazolepropionic acid (AMPA) receptors (Abe et al., 1992; Aramori and Nakanishi, 1992; Palmer et al., 1997; Snyder et al., 2001). Addition of the group I mGluR agonist DHPG led to a release of ER Ca^{2+}, with a peak amplitude of -0.07 ± 0.01 (Figure 3E and Table 1). Intriguingly, similar to 4-cmc, we also observed a significant difference in the G-CatchER$^+$ response between secondary branchpoints and secondary dendrites (-0.19 ± 0.1 versus -0.02 ± 0.01) (Figure 3F). Taken together, these findings suggest a possible selective barrier or filtering mechanism of RyR- and mGluR-dependent ER Ca^{2+} release in distal dendrites of hippocampal neurons.

G-CatchER$^+$ reports minute regional calcium-mediated events

Next, we determined if G-CatchER$^+$ could detect regional subcellular changes in Ca^{2+} signaling in the cell throughout the ER/SR network. The improved imaging resolution in HILO microscopy allows us to monitor the local Ca^{2+} responses at specific regions of interest (ROIs) throughout the entire ER/SR network. Indeed, cross-section analysis of the same region in the same cell (Figures 4A, 4C, and 4D) uncovers larger heterogeneities and variations through the ER/SR network in HILO imaging compared with that in epifluorescence imaging. When further examining two individual C2C12 cells for whole cell responses versus individual ROIs throughout the cell, we observed a variance in responses (Figure S6). When the ROIs for these two cells under HILO imaging were examined, there was a release variability of $\pm 9.6\%$ and a recovery variability of $\pm 18.9\%$ in comparison to the whole cell (Figure S6). Even when the data were normalized to initiation (t = 0 s) or to release (t = 300 s) there was still a large variance for the recovery at $\pm 12.5\%$ and $\pm 13.7\%$, respectively.

The observed heterogeneous Ca^{2+} release and recovery responses at different ROIs of cells by HILO microscopy prompted us to seek the origin of these "hotspots" of Ca^{2+} and receptor expression potentially causing this variability. It has long been speculated that "hotspots" or localized signaling regions, in the SR of skeletal muscle cells, such as C2C12 cells, are created by differential high expression of channel proteins with the capability to create Ca^{2+} concentration differences along the junctional SR, which communicate with the plasma membrane for E-C coupling (Tang et al., 2011; Launikonis et al., 2005; Rudolf et al., 2006).

To confirm whether these differences are influenced by differential ER protein distribution differences, we mapped the cellular distribution of key ER channel proteins, RyR and SERCA, using immunocytochemistry
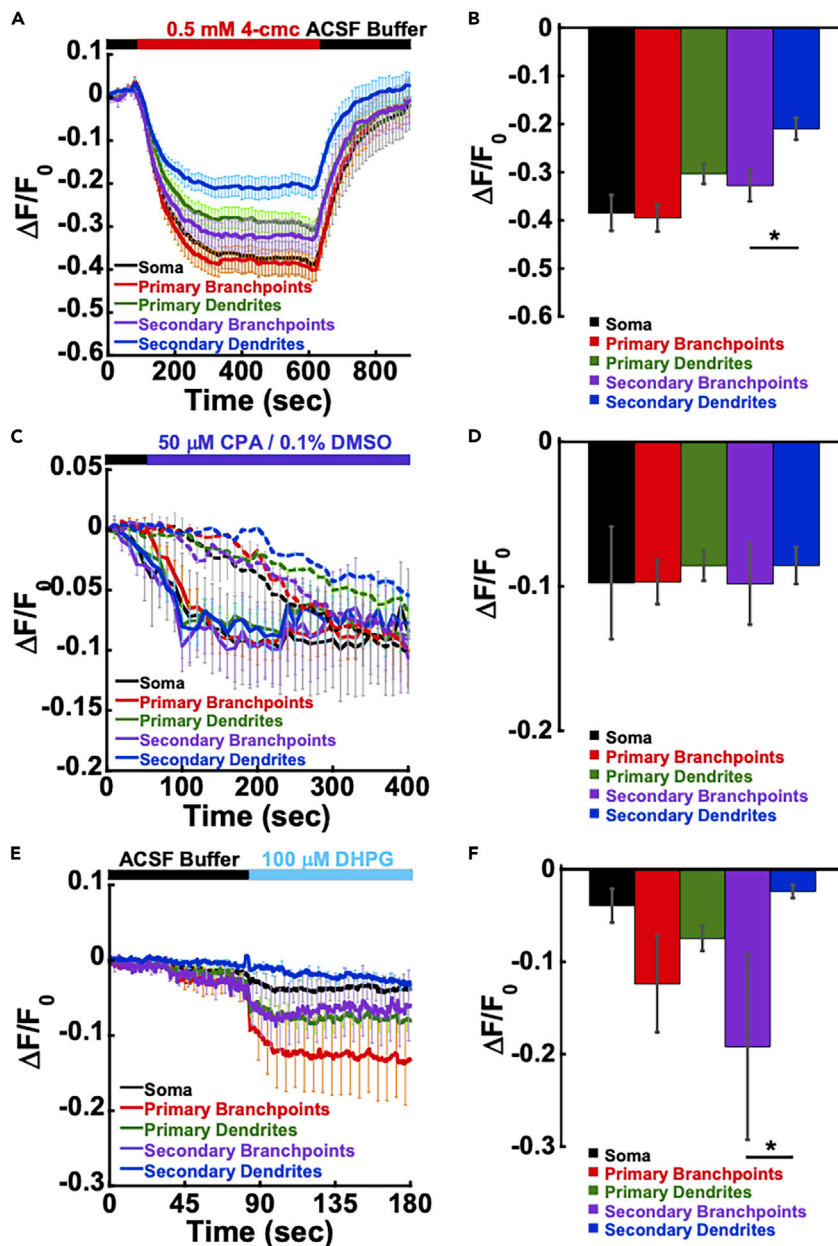
Figure 3. G-CatchER+ response in hippocampal neurons

(A) 0.5 mM of 4-cmc was added to initiate a RyR-dependent release of Ca^{2+} from the ER in mouse primary hippocampal neurons.

(B) Corresponding bar graph of 4-cmc activated Ca^{2+} release (in $\Delta F/F_0$) from the ER grouped by neuron regions. Error bars are $\pm$SEM, *p = 0.05, one-way ANOVA, Tukey's multiple comparisons.

(C) Inhibition of SERCA with 50 μM of CPA initiated a release of Ca^{2+} from the ER.

(D) Corresponding bar graph of CPA inhibited Ca^{2+} release (in $\Delta F/F_0$) from the ER grouped by neuron regions. Error bars are $\pm$SEM, one-way ANOVA, Tukey's multiple comparisons.

(E) 100 μM of DHPG was added to initiate the release of Ca^{2+} from the ER via mGluR1/5 activation in hippocampal neurons.

(F) Corresponding bar graph of DHPG-induced Ca^{2+} release (in $\Delta F/F_0$) from the ER grouped by neuron regions. Error bars are $\pm$SEM, *p = 0.02, one-way ANOVA, Tukey's multiple comparisons.
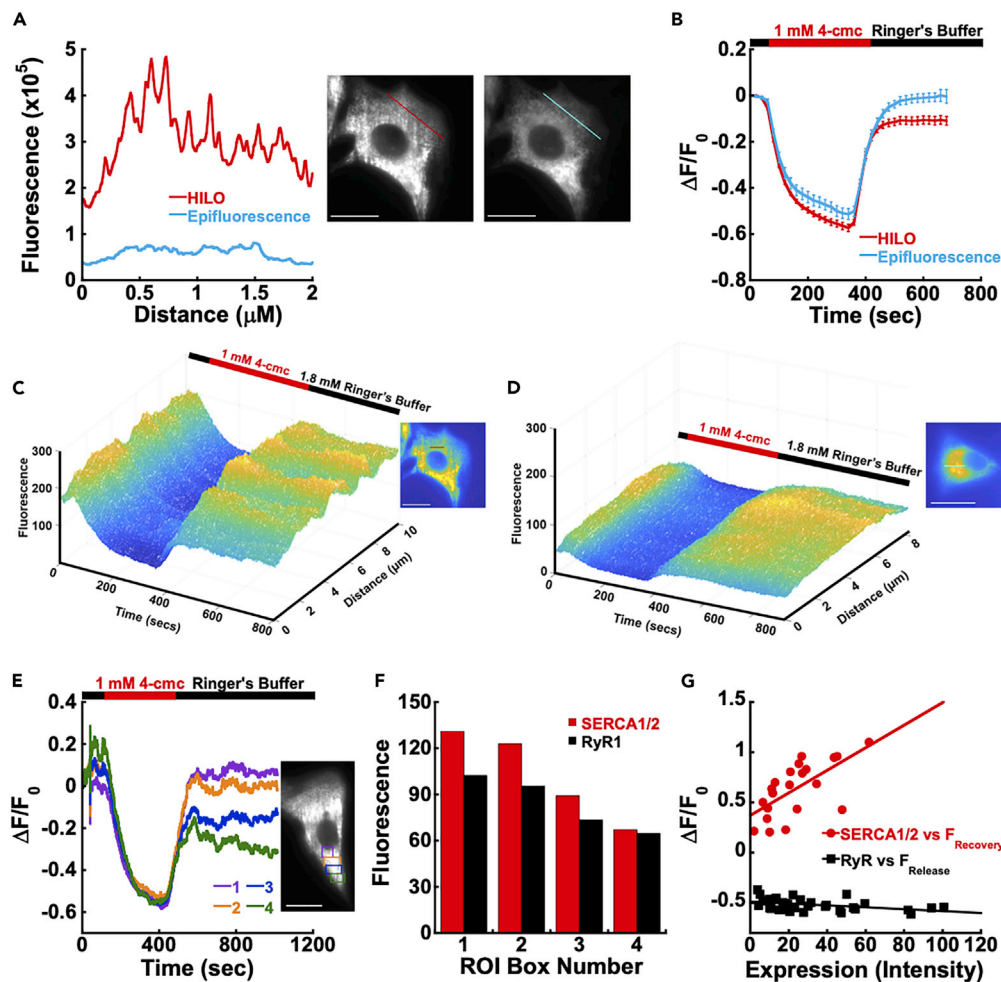
See also Figure S4.

Figure 4. G-CatchER⁺ in combination with HILO reports regional calcium-mediated events

(A) Cross-section along the same region of the cell under epifluorescence (blue) or HILO imaging (red).

(B) Average response to 1 mM 4-cmc over the same time points using HILO (red, n = 13) and epifluorescence (blue, n = 10) imaging.

(C and D) Cross section of C2C12 cells in response to 1 mM 4-cmc using HILO (C) and epifluorescence (D) imaging techniques.

(E) Release from the RyR in C2C12 cells in response to 1 mM 4-cmc in regions of interest covering the perinuclear ER (1, purple), proximal to the perinuclear ER (2, orange), proximal ER (3, blue), and distal ER (4, green).

(F) The expression of SERCA1/2 (red) and RyR1 (black) in the regions from (E).

(G) Scatterplot of SERCA1/2 (R = 0.66, n = 7) and RyR1 (R = 0.42, n = 11) expression in the perinuclear ER, proximal ER, and distal ER in each cell as a function of $\Delta F/F$ recovery and release values, respectively, in each of these regions. Scale bars, 20 μm.

See also Figure S5 and S6.

and high-resolution confocal microscopy. C2C12 cells transfected with G-CatchER⁺ were labeled with RyR1 or SERCA1 and SERCA2 together (SERCA1/2) to examine the subcellular distribution of these key ER regulators. We observed the differential expression of RyR1 in C2C12 cells that contained regions of higher expression throughout the cell with some cells having more uniform distribution and others having pockets of enhanced RyR expression (Figures S5A and S5B), whereas the distribution of SERCA1/2 were found to be highly enriched in and around the ER perinuclear region and diminishing toward the distal ER (Figures S5C and S5D).

To unambiguously verify whether reported minute Ca^{2+} dynamics is dictated by key ER-associated receptor expression, we developed a methodology that allowed us to co-register minute local Ca^{2+} dynamics by

G-CatchER$^+$ with regional ER protein expression. C2C12 cells were treated with 1 mM 4-cmc to mimic a full release of Ca^{2+} from the ER. We did not observe a significant correlation (R = 0.42) between RyR1 expression and the $\Delta F/F_0$ release (300–425 s) (Figure 4G), as the response plateaued throughout the cell (Figure 2F). In contrast, we observed a linear correlation (R = 0.66) of minute Ca^{2+} refilling dynamics with SERCA1/2 expression (Figure 4G). The expression levels of SERCA1/2 are directly related to the recovery capability of the ER in C2C12 cells. ROIs 1 (perinuclear ER) and 2 (proximal ER) have a full recovery ($\Delta F/F_0$ recovery (600–625 s)) and higher SERCA1/2 expression (Figure 4G). On the other hand, ROIs 3 and 4 (distal ER) have incomplete recovery that corelates with low expression of SERCA1/2 (Figures 4E and 4F). Taken together, the detection of minute ER Ca^{2+} dynamics dictated by localized key ER-expressed receptors is likely to play a major role in the regulation of Ca^{2+} dynamics. Targeting of G-CatchER$^+$ to regions that exhibit expression differences most likely results in response differences of key ER proteins and Ca^{2+} microdomains.

JP45-tethered G-CatchER$^+$ reports local calcium release

The existence of local Ca^{2+} microdomains in proximity to the RyR and its contributions to E-C coupling have remained controversial (Sztretye et al., 2011a, 2011b). When we examined the RyR distribution in C2C12 cells exhibiting differential formation of the myotube ($\geq$3 distinct nuclei) as well as myoblasts (1 nuclei), we found that RyR predominantly localized in myotubules, clustering on the edges of the ER (orange) (Figure S5E). Consistently, myotubule-localized RyR was significantly higher than single nuclei myoblasts by 2.8-fold, and the mature tubule was 1.9-fold higher than the forming tubule (three indistinct nuclei) (Figure S5F). JP45 is an integral protein constituent of the skeletal muscle sarcoplasmic reticulum junctional face membrane. The C terminus of JP45 is localized in the junctional SR lumen and interacts with calsequestrin (CASQ), whereas its 130-amino acid residue-long cytoplasmic domain interacts with the α-interacting domain within the loop connecting repeat I and repeat II of Ca$_v$1.1 (Anderson et al., 2003, 2006; Mosca et al., 2013; Bayley et al., 1984). To investigate the signaling dynamics in these enriched RyR regions, we fused G-CatchER$^+$ to the C terminus of JP45 to obtain the probe G-CatchER$^+$-JP45 (Figure 5). Because of its sublocalization, G-CatchER$^+$-JP45 can detect Ca^{2+} signals occurring in a domain adjacent to the junctional SR membrane encompassing the RyR calcium release channel. Wild-type mice were electroporated with G-CatchER$^+$-JP45 and G-CatchER$^+$. G-CatchER$^+$-JP45 localized to the luminal side of junctional face membrane of the terminal cisternae. In contrast, G-CatchER$^+$ localized throughout the whole lumen of the SR (Figures 5B and 5C). FDB expressing CatchER$^+$-JP45 and G-CatchER$^+$ were isolated and stimulated with a 100 Hz electrical pulse for 300 ms, and the resulting Ca^{2+} transients were recorded (Figure 5C). Fibers expressing G-CatchER$^+$-JP45 (red trace) exhibited a more rapid and larger decrease in fluorescence compared with FDB fibers expressing G-CatchER$^+$ (black trace) (Figure 5C), indicating that in the area adjacent to the lumenal domain of the RyR1, the kinetics and size of the Ca^{2+} transient are larger compared with those occurring in the whole SR. The fall time (90%–10%) of the transients for G-CatchER$^+$ and G-CatchER$^+$-JP45 are 181.8 $\pm$ 66.3 ms and 144.3 $\pm$ 81.7 ms, respectively. The peak amplitude $\Delta F/F_0$ for G-CatchER$^+$ and G-CatchER$^+$-JP45 are -0.49 ± 0.19 (n = 10 fibers from three mice) and $-0.79 \pm 0.18^*$ (n = 16 fibers from three mice *p < 0.05, Mann-Whitney test).

Similar results were obtained when immature fibers in the form of C2C12 myotubules were stimulated with 0.5 mM 4-cmc to directly activate Ca^{2+} release via RyR (Figure 5D). G-CatchER$^+$-JP45 exhibited a significantly large peak amplitude (-0.28 ± 0.01) and had a fast (88 s) Ca^{2+} release compared with those detected with G-CatchER$^+$ (-0.23 ± 0.02 and 392 s, respectively). The rise time and fall time of G-CatchER$^+$-JP45 (88 and 105 s) was 4.5-fold faster than G-CatchER$^+$.

Transgenic G-CatchER$^+$ *in vivo* analyses reveal cold-evoked Ca^{2+} release dynamics

To demonstrate the utility of G-CatchER$^+$ for *in vivo* imaging of ER/SR Ca^{2+} dynamics, we generated genetically encoded, inducible *UAS-G-CatchER$^+$* transgenic strains in *Drosophila melanogaster*. As proof-of-principle, we investigated *in vivo* G-CatchER$^+$ sensor expression and dynamics in third instar larval muscles using *Mef2^{GAL4}* to drive pan-muscle expression of *UAS-G-CatchER$^+$*. Contraction of striated skeletal muscle is initiated by a stimulus-evoked depolarization-induced influx of Ca^{2+} ions into muscle fibers. This influx of Ca^{2+} triggers a Ca^{2+}-induced Ca^{2+} release (CICR) mechanism that is critical to muscle contraction and involves Ca^{2+} release from intracellular stores (e.g. ER/SR) via the action of RyR intracellular Ca^{2+} channels (Rios, 2018). Insect studies have demonstrated that exposure to cold stimuli leads to muscle depolarization and under extended exposure, paralysis in adults referred to as chill coma (Macmillan and Sinclair, 2011; MacMillan et al., 2014). In *Drosophila* larvae, acute exposure to noxious cold stimuli elicits a nocifensive
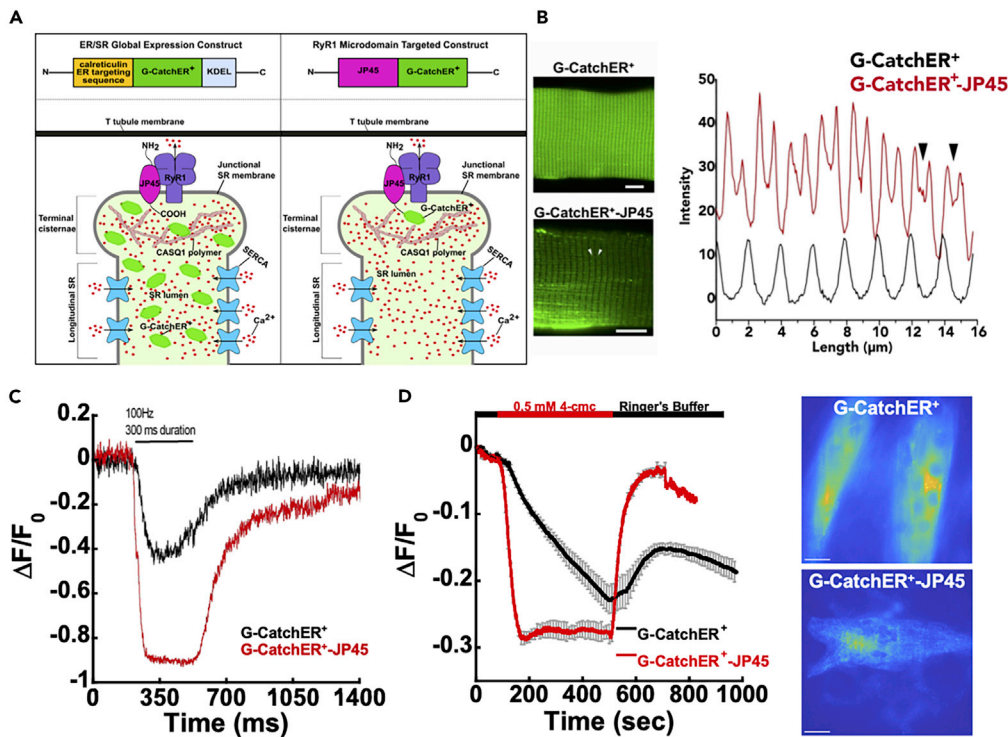
Figure 5. Monitoring global and microdomain changes in SR Ca^{2+} with globally expressed and targeted G-CatchER$^+$

(A) Representative plasmid construction and expression of globally expressed G-CatchER$^+$ and targeted G-CatchER$^+$-JP45 in the skeletal muscle SR. (Left panel) Global expression of G-CatchER$^+$. G-CatchER$^+$ contains the calreticulin signal peptide at the N terminus and the KDEL ER/SR retention sequence at the C-terminus. Resulting expression of the sensor follows a uniform distribution pattern throughout the SR monitoring global Ca^{2+}. (Right panel) RyR1 microdomain targeted G-CatchER$^+$ with JP45. G-CatchER$^+$ resides at the C-terminus of JP45. Resulting expression of the sensor positions it near the lumenal opening of RyR1 in proximity to CASQ1 polymers that establish a large proximate Ca^{2+} pool in the TC necessary for E-C coupling.

(B) Wild-type FDB fibers were transfected with G-CatchER$^+$ and G-CatchER$^+$-JP45. Images reveal differential expression patterns for the targeted and un-targeted probe. Intensity changes from G-CatchER$^+$ and G-CatchER$^+$-JP45 fibers plotted against fiber length. Arrows correspond to arrows on G-CatchER$^+$-JP45. A clear distinction is seen in the localization of G-CatchER$^+$ and G-CatchER$^+$-JP45.

(C) Ca^{2+} transients in FDB fibers were recorded upon stimulation with a 100-Hz electrical pulse for 300 ms. Black trace is fluorescence intensity monitored with G-CatchER$^+$ expressed globally, and the red trace is G-CatchER$^+$-JP45 located at the lumenal side of the junctional face membrane of the terminal cisternae.

(D) HILO imaging in C2C12 myotubule cells for G-CatchER$^+$ (black, n = 6) and G-CatchER$^+$-JP45 (red, n = 3) in response to 500-μM 4-cmc with representative cells for imaging. Scale bars, 10 μm in panel (B) and 20 μm in panel (D).

See also Figure S5.

---

full-body bilateral coordinated contraction behavior along the anteroposterior axis (Turner et al., 2016). This behavior is dependent upon neural activity of class III multi-dendritic somatosensory neurons that function as peripheral cold nociceptors (Turner et al., 2016); however it is unknown if cold-evoked larval contraction behavior correlates with Ca^{2+} release dynamics from intracellular stores in larval muscle. We hypothesized that cold exposure would elicit temperature-dependent CICR from ER/SR intracellular muscle stores. To address this hypothesis, we performed a series of *in vivo* imaging and behavioral studies using live, intact third instar *Drosophila* larvae expressing G-CatchER$^+$.

To confirm that G-CatchER$^+$ is appropriately targeted to ER/SR *in vivo*, we co-expressed G-CatchER$^+$ and the ER Sec61β translocon complex protein tagged with tdTomato in larval muscles. Consistent with C2C12 cells (Figure 2A), we observed tight co-localization of G-CatchER$^+$ with Sec61β in perinuclear regions and reticular networks of *Drosophila* larval muscles (Figure 6A). We next performed *in vivo* imaging of cold-evoked Ca^{2+} dynamics from intracellular ER/SR stores by expressing G-CatchER$^+$ in *Drosophila* larval
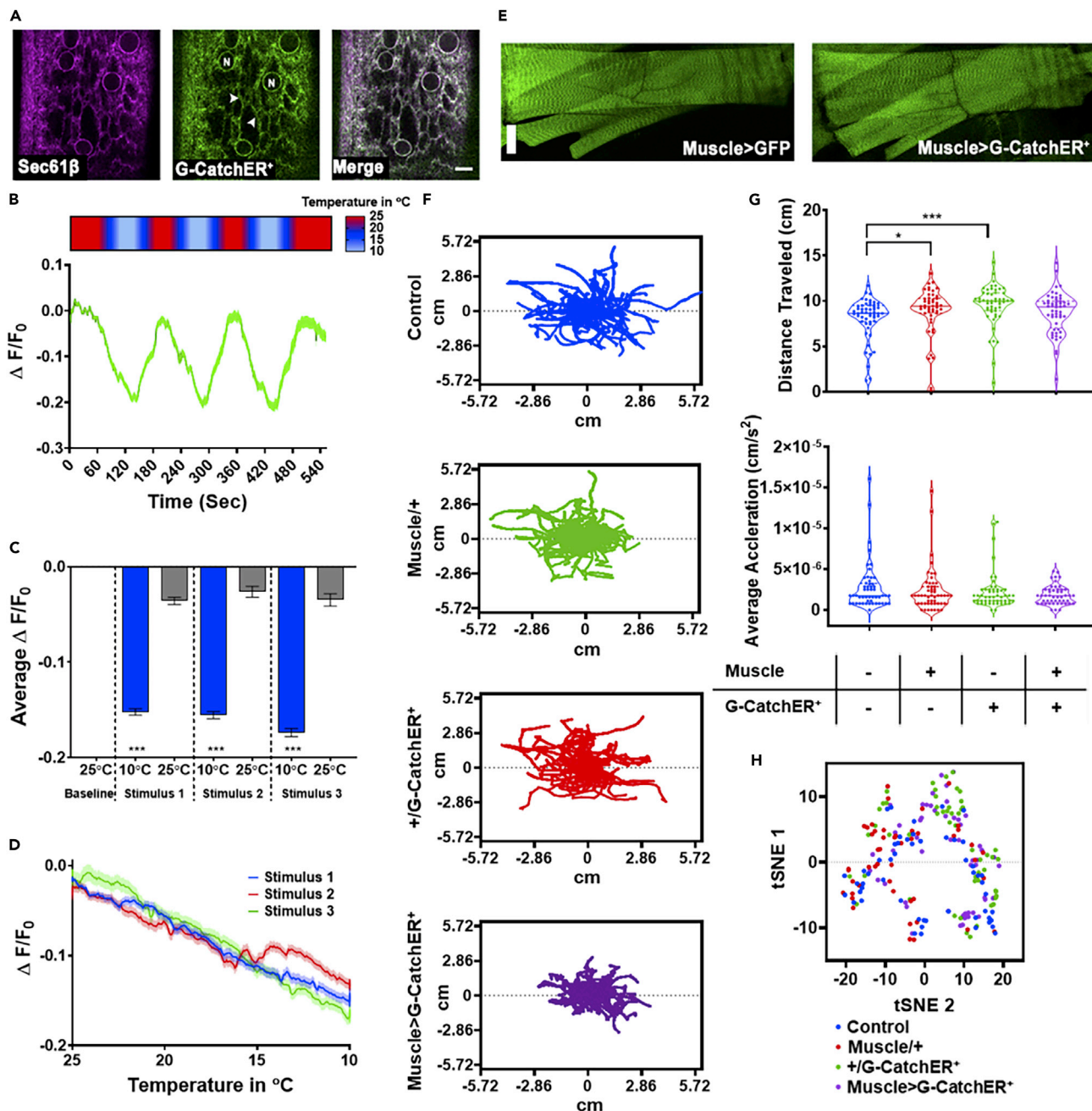
Figure 6. In vivo G-CatchER⁺ validation in *Drosophila melanogaster* larval muscles

(A) *In vivo* validation of transgenic G-CatchER⁺ expression in muscle ER/SR. The ER translocon complex protein Sec61β tagged with tdTomato (left, magenta) and G-CatchER⁺ (middle, green) exhibit tight co-localization in larval muscle characterized by perinuclear (nucleus marked by "N") and reticular network subcellular distributions (arrowheads). Genotype: *Mef2>G-CatchER⁺, Sec61β::tdTomato*. Scale bar, 10μm. Representative image from N = 10 larvae.

(B and C) Assessing cold-evoked ER/SR Ca^{2+} dynamics in muscle using G-CatchER⁺. Heatmap (B, top) shows stimulus temperature, where warmer temperatures are in red and cooler temperatures are in light blue. (B, bottom) Ca^{2+} levels reduce in response to cold stimulus, where percent change in fluorescence of G-CatchER⁺ plotted against time in seconds. Stimulus regimen details in the Methods. N = 20 animals. Error bars ±SEM. (C) Average percent change in fluorescence of G-CatchER⁺ at 25°C and 10°C, where there is a significant decrease in G-CatchER⁺ fluorescence at 10°C when compared with 25°C. Genotype: *Mef2>G-CatchER⁺*. N = 20 animals. Error bars ±SEM, ***$p < 0.0001$. Kruskal-Wallis test.

(D) Analyses of G-CatchER⁺ sensor dynamics reveal temperature-dependent increases in Ca^{2+} release across the three cold ramp stimulations with the greatest change in fluorescence at the lowest temperature (10°C).

Figure 6. Continued

(E) Expression of G-CatchER$^+$ does not grossly alter muscle morphology. (Left) Muscle cells expressing GFP and (right) muscle cells expressing G-CatchER$^+$. Genotype: *Mef2>GFP* and *Mef2>G-CatchER$^+$*. Scale bar, 50 μm. Representative image from N = 10 larvae.

(F–H) *Drosophila* larval locomotion assay to assess potential impacts of extended G-CatchER$^+$ expression on larval crawling behavior. (F) Larval locomotion tracks for individual animals during 1-min assay across various genotypes. (G, top) Distance traveled in cm and (G, bottom) average acceleration in cm/s^2. N = 48–52 animals; *p < 0.05, ***p < 0.001. Kruskal-Wallis test. (H) t-SNE analysis of multiple metrics including average distance traveled, average velocity, average acceleration, average bending, and total moving time. Iterations = 1000, perplexity = 20. (F–H) Genotype: Control (*w^{1118}*), Muscle/+ (*Mef2-GAL4* (x) *w^{1118}*), +/G-CatchER$^+$ (*UAS-G-CatchER$^+$* (x) *w^{1118}*), and Muscle > G-CatchER$^+$ (*Mef2-GAL4* (x) *UAS-G-CatchER$^+$*). N = 48–52 animals.

muscles. *Drosophila* larvae were subjected to repeated cold temperature ramps from 25°C down to 10°C (noxious) and back to 25°C coupled with live imaging of G-CatchER$^+$ fluorescence changes in muscle. Cold stimulation evoked robust Ca^{2+} release as measured by a significant reduction of ~0.15 ΔF/F$_0$ at 10°C stimulus relative to baseline 25°C and recovery to 25°C. ER/SR Ca^{2+} levels recovered consistently with repeated cold 10°C stimulus to ~0.035 ΔF/F$_0$ (Figures 6B and 6C), suggesting that sensor integrity is not notably impacted by the acute cold stimulation regimen. Moreover, analyses of G-CatchER$^+$ sensor dynamics across the full temperature ramp revealed temperature-dependent increases in Ca^{2+} release with the greatest change in fluorescence occurring at the lowest temperature (10°C) (Figure 6D). Furthermore, as G-CatchER$^+$ muscle expression is initiated by *Mef2^{GAL4}* starting from the mid-embryonic stage of development (~10 h after egg laying) and continues throughout larval development up to the end of the third instar stage (~120 h after egg laying), the observed cold-evoked Ca^{2+} release suggests long-term G-CatchER$^+$ expression does not interfere with detection of stimulus-generated intracellular Ca^{2+} store dynamics.

To further investigate potential cytotoxic effects of extended G-CatchER$^+$ expression on overall muscle architecture or tissue function, we performed morphological imaging and behavioral assays. We detected no gross morphological defects in *Drosophila* larval muscles expressing G-CatchER$^+$ relative to muscles expressing membrane-tagged GFP (Figure 6E). We then performed larval locomotion assays to assess whether extended muscle expression of G-CatchER$^+$ alters larval peristaltic crawling behavior that is dependent upon waves of muscle contraction. In general, we found no significant impairments in locomotion for G-CatchER$^+$ expressing larvae relative to wild-type and genetic background control larvae (Figures 6F–6H). No significant difference in average distance traveled or average acceleration were discovered for larvae expressing G-CatchER$^+$ compared with relevant controls (Figure 6G). Lastly, t-distributed stochastic neighbor embedding (tSNE) analysis of multiple locomotion assay variables including average distance traveled, average velocity, average acceleration, average bending, and total moving time did not reveal any distinct clusters representing any specific genotype (Figure 6H). Collectively, these *in vivo* studies reveal proper targeting of transgenically expressed G-CatchER$^+$ and identify cold-evoked ER/SR Ca^{2+} dynamics in muscle without gross impairments in muscle architecture or function based upon extended expression.

DISCUSSION

Several genetically encoded Ca^{2+} probes have been created to monitor changes in ER/SR Ca^{2+} including the Cameleon, D1ER (Palmer et al., 2004), red genetically encoded indicators for optical imaging (GECOs) such as the low-affinity sensors LAR-GECO1 (Suzuki et al., 2014b), G-CEPIA1*er* based on cfGCaMP2 (Suzuki et al., 2014b), GCaMP6-150 (de Juan-Sanz et al., 2017), and GCaMP-ER2 (Sun et al., 2019). Many of these sensors rely on CaM that contains multiple Ca^{2+} binding sites to sense Ca^{2+}, requiring a subsequent conformational change upon binding to the CaM targeting peptide such as M13. Conceptually differing from all other reported strategies, we used our innovative platform to develop next-generation classes of Ca^{2+} sensors by designing a Ca^{2+} binding site in the enhanced green fluorescent protein (EGFP) and targeting it to the ER (Tang et al., 2011). Here, our newly developed ER Ca^{2+} probe G-CatchER$^+$ exhibits improved folding and fluorescence at 37°C, which is advantageous to mammalian cells and for use *in vivo*. The introduction of mutations also increases the K$_d$ from 0.3 mM to 1.1 mM. Indeed, G-CatchER$^+$ also exhibits a much greater on-rate compared with the Ca^{2+} sensor G-CEPIA1er (Figures 1F and S2) and reports linear Ca^{2+} responses to allow a quantitative estimation of ER Ca^{2+} and dynamic changes without obscurity/limitations due to cooperativity among coupled Ca^{2+} binding sites in most reported GECIs. Using both epifluorescence and HILO microscopy, G-CatchER$^+$ quantitatively reports both channel- and receptor-mediated ER/SR Ca^{2+} transients in different cell lines and primary cells following addition of stimulatory or inhibitory agents (Figure S7). Interestingly, large variations in amplitude of 4-cmc triggered Ca^{2+} release via RyR channels in different cell types, consistent to the differential expression of RyR. On the other hand,

the IP$_3$R-mediated Ca^{2+} release have equivalent amplitudes, which is independent of cell type. Blocking ER Ca^{2+} reuptake by inhibiting SERCAs also has a small variation in the cell types analyzed (Table 1).

Using HILO microscopy to image Ca^{2+} release and recovery from small ROIs, we have revealed the 3D heterogeneous distribution of minute ER Ca^{2+} release and refilling dynamics in C2C12 cells. Such hetero-geneous release and recovery are in agreement with the expression level of RyR and SERCA1/2 concentra-tions (Figures 4G and S5). With simultaneous HILO imaging and co-staining of the same regions of these key proteins, we conclude that the heterogeneous distribution of ER Ca^{2+} release and refilling originates from the hetero-positioning and clustering of these key channel/pump proteins to form "hotspots" of Ca^{2+} dynamics. A localized ER Ca^{2+} microdomain related to stromal interaction molecule 1 (STIM1) distribution was reported using a G-CEPIA1 with SNAP$_{ER}$ tag (Luo et al., 2019). However, the expression of RyR, IP3R, and SERCA and local Ca^{2+} kinetics were not reported.

To further map the "hotspots" Ca^{2+} dynamics, we created a G-CatchER$^+$-JP45 Ca^{2+} sensor to localize it to the junctional region close to RyR1 at the lumenal site. Through analysis of the Ca^{2+} release kinetics visu-alized by locally expressed G-CatchER$^+$-JP45 compared with globally expressed G-CatchER$^+$ in the SR/ER of FDB muscle fibers upon electrostimulation, we demonstrate the local Ca^{2+} release at the membrane compartment encompassing RyR1 channel is 2.1-fold greater than global SR/ER release with much faster kinetics (Figure 5C). Such rapid Ca^{2+} release dynamics likely results from calsequestrin depolymerization caused by the drop of the lumenal SR Ca^{2+} concentration (Manno et al., 2017; Park et al., 2004). Sztretye et al. (2011b) reported a Ca^{2+} sensor D4cpv-Casq1 by fusing cameleon D4cpv with the cDNA of calseques-trin 1 or a variant that binds less Ca^{2+}. Our created sensor G-CatchER$^+$-JP45 eliminates the potential alter-ation of the ER Ca^{2+} dynamics due to expression of the Ca^{2+} buffering protein calsequestrin with multiple Ca^{2+} binding sites in the targeting sequence. Thus, it does allow unambiguous determination of the intrinsic Ca^{2+} kinetics and ER concentration that are controlled by calsequestrin.

Our direct visualization of Ca^{2+} hotspots and local microdomains close to the RyR without introducing Ca^{2+} binding proteins in a GECI has several important implications. First, the molecular mechanism of Ca^{2+} signaling is dependent on the isoforms of RyRs and SERCAs along with their cellular distributions. RyR1 is expressed in skeletal muscle and is enriched in the cerebellum, hippocampus, extraocular muscle (EOM), and diaphragm (Martin et al., 1998; Sonnleitner et al., 1998; Sekulic-Jablanovic et al., 2015). RyR2 is expressed in cardiac muscle, cerebellum, and hippocampus, as well as in human myometrial tissue (Mar-tin et al., 1998; Marx et al., 2000; Awad et al., 1997). RyR3 is expressed more broadly than RyR1 and RyR2, having been found in such regions as liver, kidney, brain, placenta, and skeletal muscle. RyR3 in the brain is found to be most highly expressed in regions such as the hippocampus, cerebellum, caudate nucleus, and amygdala, with lower expression in the thalamus, corpus callosum, and substantia nigra (Nakashima et al., 1997; Martin et al., 1998). SERCA pumps are expressed from three main genes encoding SERCA type 1–3, with SERCA1 mainly expressed in skeletal muscle and fast twitch muscle fibers and SERCA2 expressed in all tissue types, whereas SERCA3 is found mainly in non-muscle cells with minor expression in muscle cells (Hovnanian, 2007; Chemaly et al., 2018). Our developed calcium sensor will allow us to specifically probe the roles of differential subcellular Ca^{2+} dynamics in the regulation of rapid biological and pathological processes. Second, tethering our developed sensor to the ER local microdomains, which is proximal to the channel proteins, will enable us to understand molecular basis of diseases associated with ER dysfunc-tion. Malignant hyperthermia (MH), central core disease of muscle (CCD), multiminicore disease with external ophthalmoplegia (MMDO), and catecholaminergic polymorphic ventricular tachycardia (CPVT) have all been found to be related to RyR mutation and dysfunction leading to a loss in muscular and res-piratory function (Kushnir et al., 2018; Santulli et al., 2018). Both SERCA1 and 2 have disease mutations that cause Brody myopathy (BRM), acrokeratosis verruciformis (AKV), and Darier disease (DD), disorders affecting the skin and causing lesions (Hovnanian, 2007; Chemaly et al., 2018).

We found that G-CatchER$^+$ was effective in measuring ER-Ca^{2+} dynamics in primary hippocampal neurons. It is well established that the neuronal ER has a heterogeneous distribution, with its morphology becoming more complex at dendritic branchpoints (Cui-Wang et al., 2012; Spacek and Harris, 1997) that varies along the den-dritic arbor (Cui-Wang et al., 2012; Terasaki et al., 1994). The presence of ribosome studded ER in distal dendrites to allow for local protein synthesis suggests that ER-Ca^{2+} dynamics might be differentially regulated in these re-gions (Krijnse-Locker et al., 1995). Based on the data from our F$_{max}$ experiments (Figure S4E), we calculated a significant difference in concentrations of basal [Ca^{2+}] in select neuronal regions. Interestingly, treatment of

neurons with the RyR agonist 4-cmc and the group I mGluR agonist DHPG yielded a significant decrease in ER Ca^2 release between secondary branchpoints and secondary dendrites. We did not observe this effect upon treatment with CPA. The causes of the differential basal $[Ca^{2+}]$ in neuronal subregions and whether or not these also drive the heterogeneous Ca^{2+} release observed with RyR and DHPG treatment warrant future investigation. Stimulation of neurons with DHPG is known to modify ER morphology, altering the mobility of ER export and cargo (Cui-Wang et al., 2012; Aridor et al., 2004). Moreover, differential expression and neurotransmitter sensitivities of gamma aminobutyric acid (GABA) and AMPA receptors have been observed in hippocampal CA1 distal dendrites (Andrasfalvy and Magee, 2001; Pettit and Augustine, 2000), which appears to correlate with our observed differential ER-Ca^{2+} dynamics. More importantly, the distribution of key ER receptors themselves is not uniform in neurons (Blaustein and Golovina, 2001). RyRs are broadly distributed in apical dendrites, dendritic shafts, and dendritic spines (Walton et al., 1991; Segal and Korkotian, 2014), and IP$_3$Rs are localized in cell bodies, dendritic shafts, and proximal dendrites (Sharp et al., 1993). Our observation of a decrease in ER-Ca^{2+} responses in distal dendrites following DHPG is in agreement with the reported distribution pattern of the IP$_3$R. However, the significance of a RyR-mediated decrease in ER Ca^{2+} release in secondary branchpoints remains unknown. It is possible that it may be affected by the RyR isoforms that are expressed in hippocampal neurons (Sharp et al., 1993; Vlachos et al., 2009; Galeotti et al., 2008). Future experiments would be focused on determining the spatial relationships between mGluRs, RyR isoforms, and key ER-associated proteins within select neuronal regions to establish correlations with the differential spatial ER-Ca^{2+} dynamics that we observed.

We found that transgenically expressed G-CatchER$^+$ reports temperature-dependent ER/SR Ca^{2+} release/ refilling in *Drosophila* larval muscles *in vivo*. Acute exposure of *Drosophila* larvae to noxious cold stimuli is known to elicit a nocifensive full-body contraction behavior (Turner et al., 2016); however, prior to this study it was unknown how cold stimuli influence Ca^{2+} dynamics from intracellular stores in muscle to promote contractile function. We observed that cold stimulation induced significant reductions in G-CatchER$^+$ fluorescence, which recovers to near baseline levels upon cycling back to room temperature. Although future studies will be necessary to systematically interrogate the molecular mechanisms regulating cold-evoked ER/SR Ca^{2+} dynamics, these studies provide proof-of-principle evidence for the utility of G-CatchER$^+$ as an *in vivo* sensor of local dynamic Ca^{2+} transients and suggest that noxious cold-evoked larval contraction behavior may be dependent upon CICR mechanisms operating in muscle that regulate contractile function. Furthermore, we document that extended *in vivo* expression of G-CatchER$^+$ does not appear to impair stimulus-evoked Ca^{2+} dynamics nor impacts gross tissue morphology or function. Based on the vast array of tissue- and cell-type-specific *GAL4* driver transgenic strains already available, our newly reported *UAS-G-CatchER$^+$* transgenic strains can be used to study local ER/SR Ca^{2+} dynamics in a broad range of cellular and tissue contexts. For example, G-CatchER$^+$ transgenic expression could be combined with cell- or tissue-type-specific genetic disruption of putative regulators of processes such as CICR for molecular dissection. Similarly, G-CatchER$^+$ expression could be multiplexed with red fluorescent GECIs such as R-GECO or RCaMP at cell- or tissue-type specific levels to enable simultaneous high-resolution visualization of global cytosolic and subcellular compartment (e.g. ER/SR) Ca^{2+} dynamics, which could provide critical insights into spatially and/or temporally resolved Ca^{2+} signaling events.

Importantly, ER-mediated Ca^{2+} release is altered in multiple neurological disease states (Glaser et al., 2019). The IP$_3$R has three isoforms, IP$_3$R type 1–3 (Mikoshiba, 2015; Ivanova et al., 2014; Tada et al., 2016). Differential mutations in IP$_3$Rs cause multiple neurological disorders, which include spinocerebellar ataxia 15 (SCA15), spinocerebellar ataxia 29 (SCA29) (Mikoshiba, 2015; Ivanova et al., 2014; Tada et al., 2016), and Gillespie syndrome (Gerber et al., 2016; McEntagart et al., 2016). ER-mediated Ca^{2+} dysfunction has also been linked to many neurodegenerative disorders, which include Alzheimer disease (AD), Huntington disease (HD), and Parkinson disease (PD) (Bezprozvanny and Hayden, 2004; Cali et al., 2014; Magi et al., 2016; Glaser et al., 2019). The sensitivity of G-CatchER$^+$ will give researchers the ability to monitor minute changes in ER-Ca^{2+} flux in disease processes both *in vitro* and *in vivo* and will enhance our understanding of the role of regional dysfunctional ER-Ca^{2+} in neurological disease states.

Limitations of the study

Although single fluorophore fluorescence-based calcium sensors have many reported advantages over synthetic calcium dyes and FRET-based probes, there are inherent limitations that exist within this sensor that include pH sensitivity and photobleaching. This may be a limitation with G-CatchER$^+$. Future work will focus on mitigating these technical limitations. Moreover, our studies did not use this sensor in a disease model of ER dysfunction. Future work will focus on applications of this newly developed calcium probe in

uncovering the mechanism of ER dysfunction related to diseases such as central core disease, multimini-core disease, and tubular aggregate myopathy.

Resource availability

Lead contact

Further information and requests for resources and reagents should be directed to and will be fulfilled by the Lead Contact, Dr. Jenny J. Yang (jenny@gsu.edu).

Materials availability

All plasmids used in this study are available upon reasonable requests from the lead contact.

Data and code availability

All data generated or analyzed during this study will be available from the lead contact upon request.

METHODS

All methods can be found in the accompanying Transparent methods supplemental file.

SUPPLEMENTAL INFORMATION

Supplemental information can be found online at https://doi.org/10.1016/j.isci.2021.102129.

AUTHOR CONTRIBUTIONS

J.J.Y., F.N.R., C.L.M., X.D., B.D., N.F., G.G., M.A.G., A.M.M., A.A.P., D.N.C., S.T., and F.Z. designed research; F.N.R., C.L.M., X.D., B.M., B.D., A.A.P., M.A.G., C.M., G.G., S.W., T.A.R., K.M.S., R.C.T., Y.Z., J.Q., K.H., and J.L. performed research; F.N.R., C.L.M., X.D., B.M., B.D., A.A.P., M.A.G., K.M.S., Y.Z., analyzed data, and F.N.R., C.L.M., X.D., B.D., A.A.P., D.N.C., M.A.G., A.M.M., F.Z., and J.J.Y. wrote the paper.

DECLARATION OF INTERESTS

J.J.Y. is the shareholder of InLighta Biosciences. J.J.Y. is a named inventor on an issued patent (US10371708). The rest of the authors declare no competing interests.

INCLUSION AND DIVERSITY

We worked to ensure sex balance in the selection of non-human subjects. We worked to ensure diversity in experimental samples through the selection of the cell lines. One or more of the authors of this paper self-identifies as an underrepresented ethnic minority in science. One or more of the authors of this paper self-identifies as a member of the LGBTQ+ community. One or more of the authors of this paper received sup-port from a program designed to increase minority representation in science.

REFERENCES

Abe, T., Sugihara, H., Nawa, H., Shigemoto, R., Mizuno, N., and Nakanishi, S. (1992). Molecular characterization of a novel metabotropic glutamate receptor mGluR5 coupled to inositol phosphate/Ca2+ signal transduction. J. Biol. Chem. *267*, 13361–13368.

Anderson, A.A., Altafaj, X., Zheng, Z., Wang, Z.M., Delbono, O., Ronjat, M., Treves, S., and Zorzato, F. (2006). The junctional SR protein JP-45 affects the functional expression of the voltage-dependent Ca2+ channel Cav1.1. J. Cell Sci. *119*, 2145–2155.

Anderson, A.A., Treves, S., Biral, D., Betto, R., Sandona, D., Ronjat, M., and Zorzato, F. (2003). The novel skeletal muscle sarcoplasmic reticulum JP-45 protein. Molecular cloning, tissue distribution, developmental expression, and interaction with alpha 1.1 subunit of the voltage-gated calcium channel. J. Biol. Chem. *278*, 39987–39992.

Andrasfalvy, B.K., and Magee, J.C. (2001). Distance-dependent increase in AMPA receptor number in the dendrites of adult hippocampal CA1 pyramidal neurons. J. Neurosci. *21*, 9151–9159.

Aramori, I., and Nakanishi, S. (1992). Signal transduction and pharmacological characteristics of a metabotropic glutamate receptor, mGluR1, in transfected CHO cells. Neuron *8*, 757–765.

Aridor, M., Guzik, A.K., Bielli, A., and Fish, K.N. (2004). Endoplasmic reticulum export site formation and function in dendrites. J. Neurosci. *24*, 3770–3776.

Awad, S.S., Lamb, H.K., Morgan, J.M., Dunlop, W., and Gillespie, J.I. (1997). Differential expression of ryanodine receptor RyR2 mRNA in the non-pregnant and pregnant human myometrium. Biochem. J. *322*, 777–783.

Bayley, P., Ahlstrom, P., Martin, S.R., and Forsen, S. (1984). The kinetics of calcium-binding to calmodulin - Quin-2 and ans stopped-flow fluorescence studies. Biochem. Biophys. Res. Commun. *120*, 185–191.

Berridge, M.J. (2002). The endoplasmic reticulum: a multifunctional signaling organelle. Cell Calcium *32*, 235–249.

Berridge, M.J., Bootman, M.D., and Roderick, H.L. (2003). Calcium signalling: dynamics, homeostasis and remodelling. Nat. Rev. Mol. Cell Biol. *4*, 517–529.

Bezprozvanny, I., and Hayden, M.R. (2004). Deranged neuronal calcium signaling and Huntington disease. Biochem. Biophys. Res. Commun. *322*, 1310–1317.

Blaustein, M.P., and Golovina, V.A. (2001). Structural complexity and functional diversity of endoplasmic reticulum Ca(2+) stores. Trends Neurosci. *24*, 602–608.

Bourne, J.N., and Harris, K.M. (2012). Nanoscale analysis of structural synaptic plasticity. Curr. Opin. Neurobiol. *22*, 372–382.

Cali, T., Ottolini, D., and Brini, M. (2014). Calcium signaling in Parkinson's disease. Cell Tissue Res. *357*, 439–454.

Chemaly, E.R., Troncone, L., and Lebeche, D. (2018). SERCA control of cell death and survival. Cell Calcium *69*, 46–61.

Citri, A., and Malenka, R.C. (2008). Synaptic plasticity: multiple forms, functions, and mechanisms. Neuropsychopharmacology *33*, 18–41.

Clapham, D.E. (2007). Calcium signaling. Cell *131*, 1047–1058.

Cui-Wang, T., Hanus, C., Cui, T., Helton, T., Bourne, J., Watson, D., Harris, K.M., and Ehlers, M.D. (2012). Local zones of endoplasmic reticulum complexity confine cargo in neuronal dendrites. Cell *148*, 309–321.

de Juan-Sanz, J., Holt, G.T., Schreiter, E.R., De Juan, F., Kim, D.S., and Ryan, T.A. (2017). Axonal endoplasmic reticulum Ca(2+) content controls release Probability in CNS nerve terminals. Neuron *93*, 867–881 e6.

Galeotti, N., Vivoli, E., Bartolini, A., and Ghelardini, C. (2008). A gene-specific cerebral types 1, 2, and 3 RyR protein knockdown induces an antidepressant-like effect in mice. J. Neurochem. *106*, 2385–2394.

Gerber, S., Alzayady, K.J., Burglen, L., Bremond-Gignac, D., Marchesin, V., Roche, O., Rio, M., Funalot, B., Calmon, R., Durr, A., et al. (2016). Recessive and dominant de novo ITPR1 mutations cause Gillespie syndrome. Am. J. Hum. Genet. *98*, 971–980.

Glaser, T., Arnaud Sampaio, V.F., Lameu, C., and Ulrich, H. (2019). Calcium signalling: a common target in neurological disorders and neurogenesis. Semin. Cell Dev. Biol. *95*, 25–33.

Hovnanian, A. (2007). SERCA pumps and human diseases. Subcell Biochem. *45*, 337–363.

Ivanova, H., Vervliet, T., Missiaen, L., Parys, J.B., De Smedt, H., and Bultynck, G. (2014). Inositol 1,4,5-trisphosphate receptor-isoform diversity in cell death and survival. Biochim. Biophys. Acta *1843*, 2164–2183.

Jimenez-Moreno, R., Wang, Z.M., Messi, M.L., and Delbono, O. (2010). Sarcoplasmic reticulum Ca2+ depletion in adult skeletal muscle fibres measured with the biosensor D1ER. Pflugers Arch. *459*, 725–735.

Kabbara, A.A., and Allen, D.G. (2001). The use of the indicator fluo-5N to measure sarcoplasmic reticulum calcium in single muscle fibres of the cane toad. J. Physiol. *534*, 87–97.

Krijnse-Locker, J., Parton, R.G., Fuller, S.D., Griffiths, G., and Dotti, C.G. (1995). The organization of the endoplasmic reticulum and the intermediate compartment in cultured rat hippocampal neurons. Mol. Biol. Cell *6*, 1315–1332.

Kushnir, A., Wajsberg, B., and Marks, A.R. (2018). Ryanodine receptor dysfunction in human disorders. Biochim. Biophys. Acta Mol. Cell Res. *1865*, 1687–1697.

Landolfi, B., Curci, S., Debellis, L., Pozzan, T., and Hofer, A.M. (1998). Ca2+ homeostasis in the agonist-sensitive internal store: functional interactions between mitochondria and the ER measured in situ in intact cells. J. Cell Biol. *142*, 1235–1243.

Launikonis, B.S., Zhou, J., Royer, L., Shannon, T.R., Brum, G., and Rios, E. (2005). Confocal imaging of [Ca2+] in cellular organelles by SEER, shifted excitation and emission ratioing of fluorescence. J. Physiol. *567*, 523–543.

Luo, C., Wang, H., Liu, Q., He, W., Yuan, L., and Xu, P. (2019). A genetically encoded ratiometric calcium sensor enables quantitative measurement of the local calcium microdomain in the endoplasmic reticulum. Biophys. Rep. *5*, 31–42.

MacMillan, H.A., Findsen, A., Pedersen, T.H., and Overgaard, J. (2014). Cold-induced depolarization of insect muscle: differing roles of extracellular K+ during acute and chronic chilling. J. Exp. Biol. *217*, 2930–2938.

Macmillan, H.A., and Sinclair, B.J. (2011). Mechanisms underlying insect chill-coma. J. Insect Physiol. *57*, 12–20.

Magi, S., Castaldo, P., Macri, M.L., Maiolino, M., Matteucci, A., Bastioli, G., Gratteri, S., Amoroso, S., and Lariccia, V. (2016). Intracellular calcium dysregulation: implications for alzheimer's disease. Biomed. Res. Int. *2016*, 6701324.

Manno, C., Figueroa, L.C., Gillespie, D., Fitts, R., Kang, C., Franzini-Armstrong, C., and Rios, E. (2017). Calsequestrin depolymerizes when calcium is depleted in the sarcoplasmic reticulum of working muscle. Proc. Natl. Acad. Sci. U S A *114*, E638–E647.

Martin, C., Chapman, K.E., Seckl, J.R., and Ashley, R.H. (1998). Partial cloning and differential expression of ryanodine receptor/calcium-release channel genes in human tissues including the hippocampus and cerebellum. Neuroscience *85*, 205–216.

Marx, S.O., Reiken, S., Hisamatsu, Y., Jayaraman, T., Burkhoff, D., Rosemblit, N., and Marks, A.R. (2000). PKA phosphorylation dissociates FKBP12.6 from the calcium release channel (ryanodine receptor): defective regulation in failing hearts. Cell *101*, 365–376.

McEntagart, M., Williamson, K.A., Rainger, J.K., Wheeler, A., Seawright, A., De Baere, E., Verdin, H., Bergendahl, L.T., Quigley, A., Rainger, J., et al. (2016). A restricted repertoire of de novo mutations in ITPR1 cause Gillespie syndrome with evidence for dominant-negative effect. Am. J. Hum. Genet. *98*, 981–992.

Melzer, W., Rios, E., and Schneider, M.F. (1987). A general procedure for determining the rate of calcium release from the sarcoplasmic reticulum in skeletal muscle fibers. Biophys. J. *51*, 849–863.

Mikoshiba, K. (2015). Role of IP3 receptor signaling in cell functions and diseases. Adv. Biol. Regul. *57*, 217–227.

Miyawaki, A., Llopis, J., Heim, R., Mccaffery, J.M., Adams, J.A., Ikura, M., and Tsien, R.Y. (1997). Fluorescent indicators for Ca2+ based on green fluorescent proteins and calmodulin. Nature *388*, 882–887.

Mosca, B., Delbono, O., Laura Messi, M., Bergamelli, L., Wang, Z.M., Vukcevic, M., Lopez, R., Treves, S., Nishi, M., Takeshima, H., et al. (2013). Enhanced dihydropyridine receptor calcium channel activity restores muscle strength in JP45/CASQ1 double knockout mice. Nat. Commun. 4, 1541.

Nakashima, Y., Nishimura, S., Maeda, A., Barsoumian, E.L., Hakamata, Y., Nakai, J., Allen, P.D., Imoto, K., and Kita, T. (1997). Molecular cloning and characterization of a human brain ryanodine receptor. FEBS Lett. 417, 157–162.

Palmer, A.E., Jin, C., Reed, J.C., and Tsien, R.Y. (2004). Bcl-2-mediated alterations in endoplasmic reticulum Ca2+ analyzed with an improved genetically encoded fluorescent sensor. Proc. Natl. Acad. Sci. U S A 101, 17404–17409.

Palmer, M.J., Irving, A.J., Seabrook, G.R., Jane, D.E., and Collingridge, G.L. (1997). The group I mGlu receptor agonist DHPG induces a novel form of LTD in the CA1 region of the hippocampus. Neuropharmacology 36, 1517–1532.

Papp, S., Dziak, E., Michalak, M., and Opas, M. (2003). Is all of the endoplasmic reticulum created equal? The effects of the heterogeneous distribution of endoplasmic reticulum Ca2+-handling proteins. J. Cell Biol. 160, 475–479.

Park, H., Park, I.Y., Kim, E., Youn, B., Fields, K., Dunker, A.K., and Kang, C. (2004). Comparing skeletal and cardiac calsequestrin structures and their calcium binding: a proposed mechanism for coupled calcium binding and protein polymerization. J. Biol. Chem. 279, 18026–18033.

Pedelacq, J.D., Cabantous, S., Tran, T., Terwilliger, T.C., and Waldo, G.S. (2006). Engineering and characterization of a superfolder green fluorescent protein. Nat. Biotechnol. 24, 79–88.

Petersen, O.H., Tepikin, A., and Park, M.K. (2001). The endoplasmic reticulum: one continuous or several separate Ca2+ stores? Trends Neurosci. 24, 271–276.

Pettit, D.L., and Augustine, G.J. (2000). Distribution of functional glutamate and GABA receptors on hippocampal pyramidal cells and interneurons. J. Neurophysiol. 84, 28–38.

Rios, E. (2018). Calcium-induced release of calcium in muscle: 50 years of work and the emerging consensus. J. Gen. Physiol. 150, 521–537.

Rudolf, R., Magalhaes, P.J., and Pozzan, T. (2006). Direct in vivo monitoring of sarcoplasmic reticulum Ca2+ and cytosolic cAMP dynamics in mouse skeletal muscle. J. Cell Biol. 173, 187–193.

Santulli, G., Lewis, D., Des Georges, A., Marks, A.R., and Frank, J. (2018). Ryanodine receptor structure and function in health and disease. Subcell Biochem. 87, 329–352.

Schneider, M.F., Simon, B.J., and Szucs, G. (1987). Depletion of calcium from the sarcoplasmic reticulum during calcium release in frog skeletal muscle. J. Physiol. 392, 167–192.

Segal, M., and Korkotian, E. (2014). Endoplasmic reticulum calcium stores in dendritic spines. Front. Neuroanat. 8, 64.

Sekulic-Jablanovic, M., Palmowski-Wolfe, A., Zorzato, F., and Treves, S. (2015). Characterization of excitation–contraction coupling components in human extraocular muscles. Biochem. J. 466, 29–36.

Sharp, A.H., Mcpherson, P.S., Dawson, T.M., Aoki, C., Campbell, K.P., and Snyder, S.H. (1993). Differential immunohistochemical localization of inositol 1,4,5-trisphosphate- and ryanodine-sensitive Ca2+ release channels in rat brain. J. Neurosci. 13, 3051–3063.

Siemering, K.R., Golbik, R., Sever, R., and Haseloff, J. (1996). Mutations that suppress the thermosensitivity of green fluorescent protein. Curr. Biol. 6, 1653–1663.

Snyder, E.M., Philpot, B.D., Huber, K.M., Dong, X., Fallon, J.R., and Bear, M.F. (2001). Internalization of ionotropic glutamate receptors in response to mGluR activation. Nat. Neurosci. 4, 1079–1085.

Sonnleitner, A., Conti, A., Bertocchini, F., Schindler, H., and Sorrentino, V.J.T.E.J. (1998). Functional properties of the ryanodine receptor type 3 (RyR3) Ca2+ release channel. EMBO J. 17, 2790–2798.

Spacek, J., and Harris, K.M. (1997). Three-dimensional organization of smooth endoplasmic reticulum in hippocampal CA1 dendrites and dendritic spines of the immature and mature rat. J. Neurosci. 17, 190–203.

Sun, C., Shui, B., Zhao, W., Liu, H., Li, W., Lee, J.C., Doran, R., Lee, F.K., Sun, T., Shen, Q.S., et al. (2019). Central role of IP3R2-mediated Ca(2+) oscillation in self-renewal of liver cancer stem cells elucidated by high-signal ER sensor. Cell Death Dis. 10, 396.

Suzuki, J., Kanemaru, K., Ishii, K., Ohkura, M., Okubo, Y., and Iino, M. (2014a). Imaging intraorganellar Ca2+ at subcellular resolution using CEPIA. Nat. Commun. 5, 4153.

Suzuki, S., Kuenen, J.G., Schipper, K., Van Der Velde, S., Ishii, S., Wu, A., Sorokin, D.Y., Tenney, A., Meng, X., Morrill, P.L., et al. (2014b). Physiological and genomic features of highly alkaliphilic hydrogen-utilizing Betaproteobacteria from a continental serpentinizing site. Nat. Commun. 5, 3900.

Sztretye, M., Yi, J., Figueroa, L., Zhou, J., Royer, L., Allen, P., Brum, G., and Rios, E. (2011a). Measurement of RyR permeability reveals a role of calsequestrin in termination of SR Ca(2+) release in skeletal muscle. J. Gen. Physiol. 138, 231–247.

Sztretye, M., Yi, J., Figueroa, L., Zhou, J., Royer, L., and Rios, E. (2011b). D4cpv-calsequestrin: a sensitive ratiometric biosensor accurately targeted to the calcium store of skeletal muscle. J. Gen. Physiol. 138, 211–229.

Tada, M., Nishizawa, M., and Onodera, O. (2016). Roles of inositol 1,4,5-trisphosphate receptors in spinocerebellar ataxias. Neurochem. Int. 94, 1–8.

Tang, S., Deng, X., Jiang, J., Kirberger, M., and Yang, J.J. (2020). Design of calcium-binding proteins to sense calcium. Molecules 25, 2148.

Tang, S., Reddish, F., Zhuo, Y., and Yang, J.J. (2015). Fast kinetics of calcium signaling and sensor design. Curr. Opin. Chem. Biol. 27, 90–97.

Tang, S., Wong, H.C., Wang, Z.M., Huang, Y., Zou, J., Zhuo, Y., Pennati, A., Gadda, G., Delbono, O., and Yang, J.J. (2011). Design and application of a class of sensors to monitor Ca(2+) dynamics in high Ca(2+) concentration cellular compartments. Proc. Natl. Acad. Sci. U S A 108, 16265–16270.

Terasaki, M., Slater, N.T., Fein, A., Schmidek, A., and Reese, T.S. (1994). Continuous network of endoplasmic reticulum in cerebellar Purkinje neurons. Proc. Natl. Acad. Sci. U S A 91, 7510–7514.

Tokunaga, M., Imamoto, N., and Sakata-Sogawa, K. (2008). Highly inclined thin illumination enables clear single-molecule imaging in cells. Nat. Methods 5, 159–161.

Turner, H.N., Armengol, K., Patel, A.A., Himmel, N.J., Sullivan, L., Iyer, S.C., Bhattacharya, S., Iyer, E.P.R., Landry, C., Galko, M.J., and Cox, D.N. (2016). The TRP channels Pkd2, NompC, and trpm act in cold-sensing neurons to mediate unique aversive behaviors to noxious cold in Drosophila. Curr. Biol. 26, 3116–3128.

Vlachos, A., Korkotian, E., Schonfeld, E., Copanaki, E., Deller, T., and Segal, M. (2009). Synaptopodin regulates plasticity of dendritic spines in hippocampal neurons. J. Neurosci. 29, 1017–1033.

Walton, P.D., Airey, J.A., Sutko, J.L., Beck, C.F., Mignery, G.A., Sudhof, T.C., Deerinck, T.J., and Ellisman, M.H. (1991). Ryanodine and inositol trisphosphate receptors coexist in avian cerebellar Purkinje neurons. J. Cell Biol. 113, 1145–1157.

Zhuo, Y., Solntsev, K.M., Reddish, F., Tang, S., and Yang, J.J. (2015). Effect of Ca(2)(+) on the steady-state and time-resolved emission properties of the genetically encoded fluorescent sensor CatchER. J. Phys. Chem. B 119, 2103–2111.

Supplemental information

Rapid subcellular calcium

responses and dynamics

by calcium sensor G-CatchER$^+$

Florence N. Reddish, Cassandra L. Miller, Xiaonan Deng, Bin Dong, Atit A. Patel, Mohammad A. Ghane, Barbara Mosca, Cheyenne McBean, Shengnan Wu, Kyril M. Solntsev, You Zhuo, Giovanni Gadda, Ning Fang, Daniel N. Cox, Angela M. Mabb, Susan Treves, Francesco Zorzato, and Jenny J. Yang

Supplemental figures and Tables
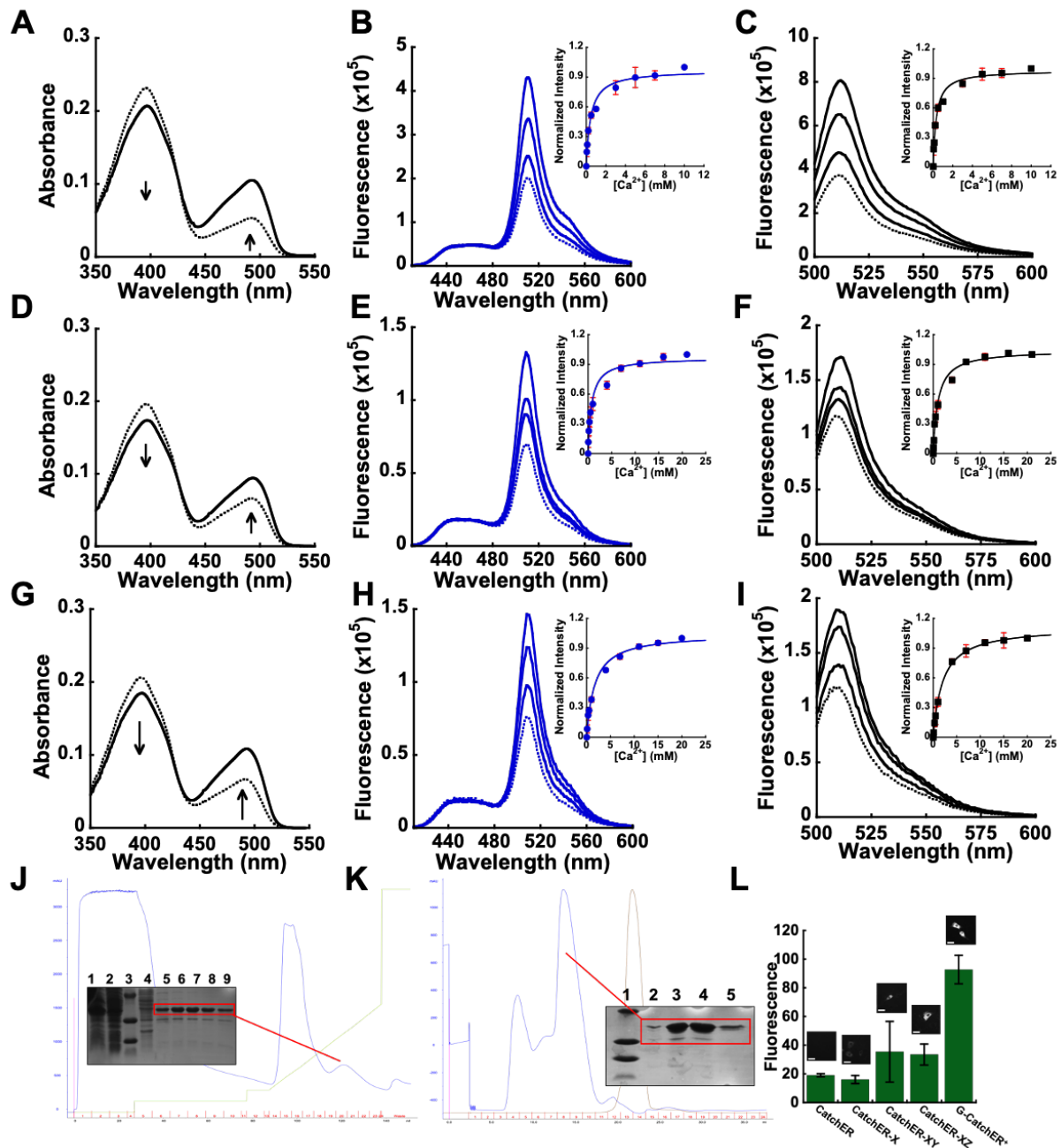
Supplemental Figure 1. In vitro Ca^{2+} K$_d$ and purification of bacterially expressed of CatchER-X (S175G mutation), CatchER-XY (S175G and Y39N mutation) and G-CatchER-XZ (S175G and S30R mutation) variants using fluorescence spectroscopy, related to Figure 1.

Inset, Binding curves were fit with a 1:1 binding equation to obtain the K$_d$. **A, D, G.** Absorbance spectra of the protein samples before Ca^{2+} titration (dashed line) and after with a saturating amount of Ca^{2+} (solid line). **B** and **C**. Fluorescence increase of S175G in response to 0-7 mM Ca^{2+}. **E** and **F**. Fluorescence increase of S175G S30R in response to 0-10 mM Ca^{2+}. **H** and **I**. Fluorescence increase of S175G Y39N in response to 0-21 mM Ca^{2+}. **J.** HisTag purification of G-CatchER$^+$. Inset SDS-PAGE gel shows samples from different stages of purification. **K.** Size exclusion chromatography of G-CatchER$^+$ using a Superdex 200 column. Inset SDS-PAGE gel shows pure fractions of G-CatchER$^+$ peak in red box corresponding to the chromatogram peak. **L.** Fluorescence intensity plot at 37°C for CatchER, CatchER-X (S175G mutation), CatchER-XY (S175G and Y39N mutation), G-CatchER-XZ (S175G and S30R mutation), and G-CatchER$^+$ (S175G, Y39N and S30R mutations) in C2C12 cells. Scale bars, 20 µm.
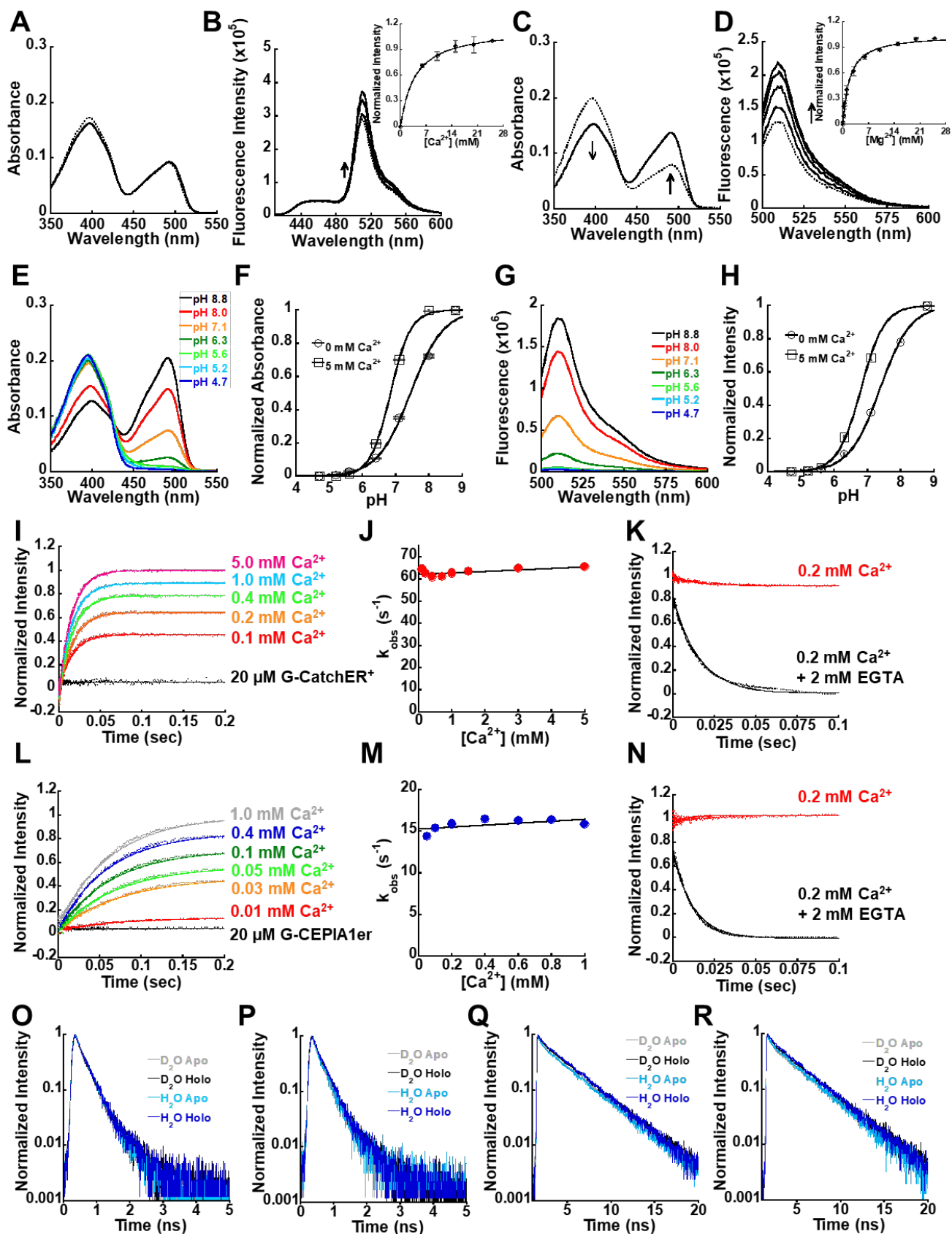
Supplemental Figure 2. Optical properties and fluorescence lifetime of G-CatchER⁺, and Ca²⁺ binding kinetics of G-CatchER⁺ and G-CEPIA1er, related to Figure 1.

A. Absorbance spectra of 10 μM G-CatchER⁺ in 10 mM Tris pH 7.4 with 150 mM KCl before (dashed line) and after titrating up to 25 mM Ca^{2+} (solid line). **B.** Fluorescence increase of G-CatchER⁺ in response to the stepwise addition of up to 25 mM Ca^{2+} in high salt buffer excited at 395 nm monitored at 510 nm emission. *Inset.* Fitting of the normalized fluorescence intensity. The Ca^{2+} K_d in the presence of 150 mM KCl was 3.74 ± 0.70 mM. **C.** Absorbance spectra of 10 μM G-CatchER⁺ sample in 10 mM Tris pH 7.4 before (dashed line) and after (solid line) titrating u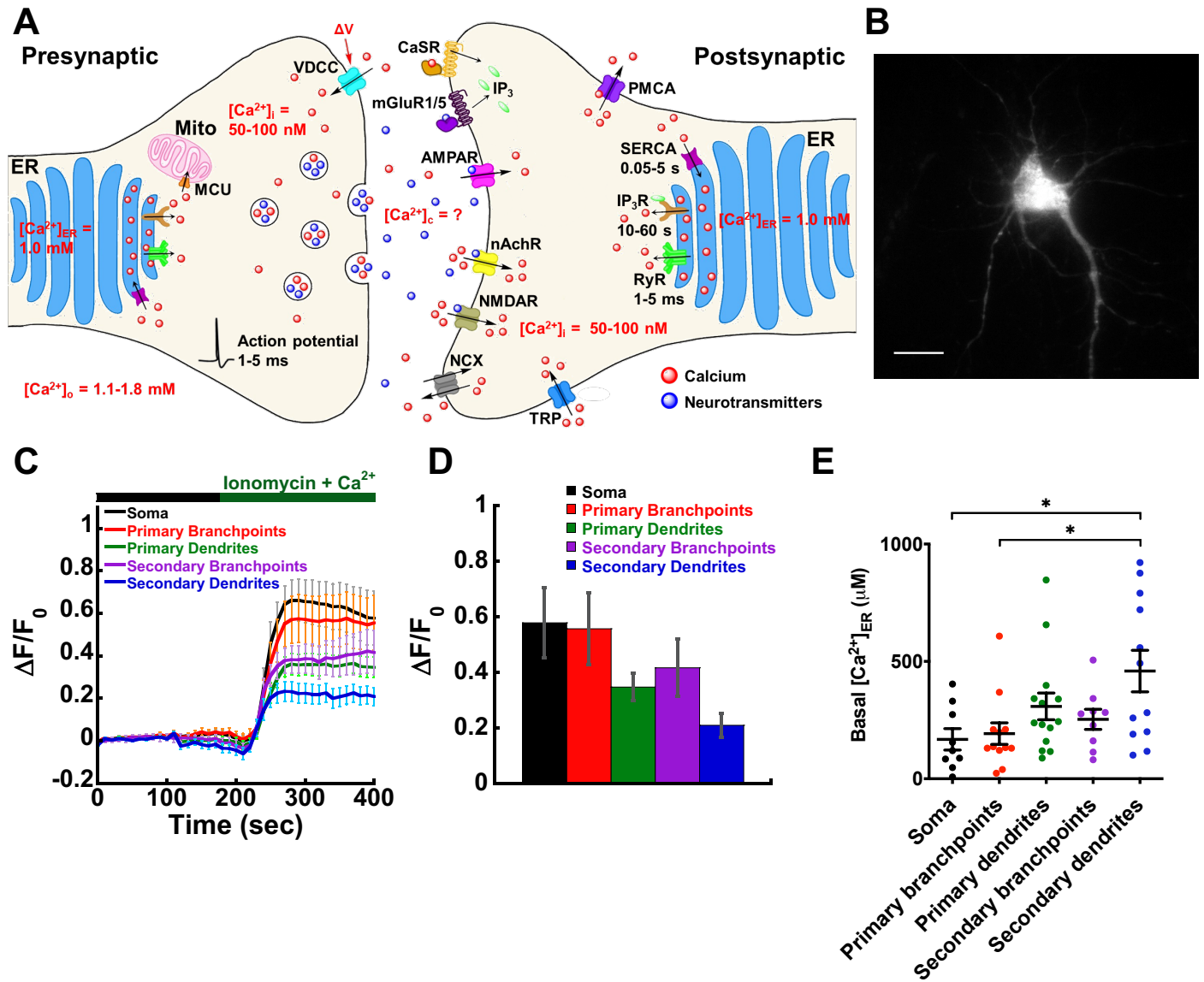p to 25 mM Mg^{2+}. **D.** Fluorescence increase of G-CatchER⁺ in response to the stepwise addition of up to 25 mM Mg^{2+} in 10 mM Tris pH 7.4 excited at 488 nm monitored at 510 nm emission. *Inset.* Fitting of the normalized fluorescence intensity. Mg^{2+} K_d was 1.78 ± 0.44 mM. **E-H**. The chromophore pK_a of G-CatchER⁺ was measured by absorbance and fluorescence spectroscopy in the absence and presence of 5 mM Ca^{2+}. **E.** Representative absorbance spectra of G-CatchER⁺ in the absence of Ca^{2+}. **F.** Normalized 488 nm absorbance data in the absence (●) and presence (■) of 5 mM Ca^{2+}. The calculated pK_a was 7.4 ± 0.0 without Ca^{2+} and 6.8 ± 0.0 with 5 mM Ca^{2+}. **G.** Representative fluorescence spectra of G-CatchER⁺ in the absence of Ca^{2+} using 488 nm excitation with emission at 510 nm. **H.** Normalized fluorescence intensity data in the absence (●) and presence (■) of 5 mM Ca^{2+}. Calculated pK_a was 7.4 ± 0.0 without Ca^{2+} and 6.8 ± 0.0 with 5 mM Ca^{2+}. **I.** Normalized fluorescence intensity of Ca^{2+} associated kinetics of G-CatchER⁺ in the presence of different concentrations of Ca^{2+}. **J.** k_{obs} under different concentrations of Ca^{2+}, fitted by a linear curve. **K.** Normalized fluorescence intensity of Ca^{2+} disassociation kinetics of G-CatchER⁺ in the presence of 2 mM EGTA. **L.** Normalized fluorescence intensity of Ca^{2+} association kinetics of G-CEPIA1er in the presence of different concentrations of Ca^{2+}. **M.** k_{obs} under different concentrations of Ca^{2+}, fitted by a linear curve. **N.** Normalized fluorescence intensity of Ca^{2+} dissociation kinetics of G-CatchER⁺ in the presence of 2 mM EGTA. **O&P.** G-CatchER **(O)** and G-CatchER⁺ **(P)** were excited at 372 nm and emitted at 440 nm in the time range of 5 ns. **Q&R.** G-CatchER **(Q)** and G-CatchER⁺**(R)** were excited at 372 nm and emitted at 510 nm in the time range of 20 ns.
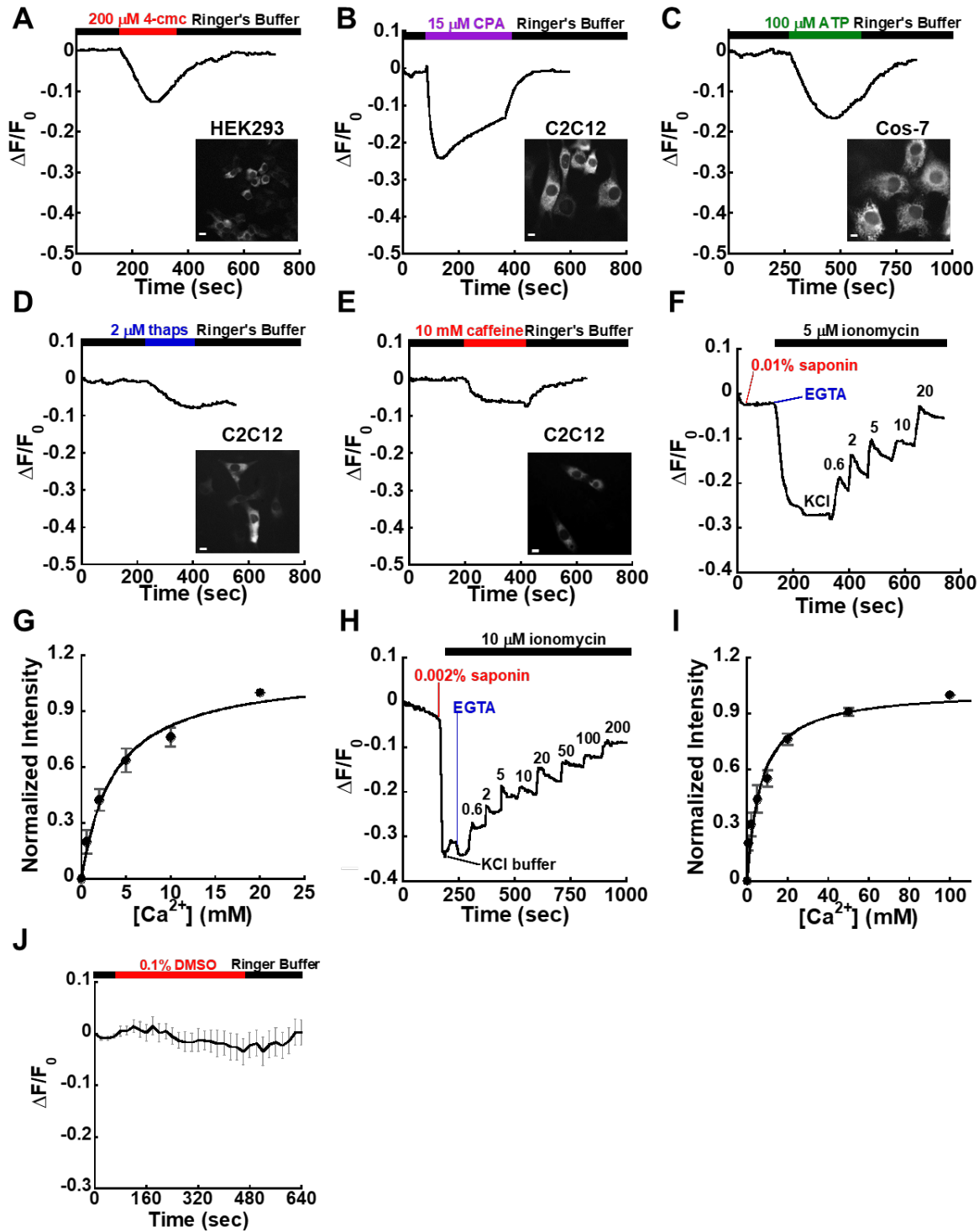
Supplemental Figure 3. *In Situ* **validation of G-CatchER⁺ in response to receptor agonists and antagonists in several cell lines, related to Table 1 and Figure 2.**
Representative data plots from cell studies of G-CatchER⁺ responses to changes in ER Ca²⁺. **A.** RyR mediated Ca²⁺ release from the ER in HEK293 cells using 4-cmc. **B.** Reversible inhibition of SERCA pump in C2C12 cells using 15 µM of CPA. ER Ca²⁺ is temporarily reduced by blocking SERCA pump function. **C.** 100 µM of ATP was added to initiate a release of Ca²⁺ from the ER in Cos-7 cells. ATP acts on the IP₃R, which indirectly releases Ca²⁺ from the ER after production of IP₃ from P2YR activation. **D.** Irreversible SERCA pump inhibition with 2 µM

thapsigargin in C2C12 cells. After addition of thapsigargin and washing with Ringer's buffer, no ER refilling occurs. E. RyR1 activation with 10 mM caffeine in C2C12 cells. **F-I**. Measurement of the *in situ* K_d of G-CatchER$^+$ in Cos7 (**F** and **G**) and HEK293 cells (**H** and **I**). **F.** 0, 0.6, 2, 6, 10, and 20 mM Ca^{2+} was added to permeabilized Cos7 cells in the presence of 5 μM ionomycin. n = 11. **G.** Intensity from **F** was normalized and fitted with the 1:1 binding equation to get an *in situ* Ca^{2+} K_d of 3.84 ± 1.48 mM. **H.** 0.6, 2, 5, 10, 20, 50, 100, and 200 mM Ca^{2+} was added to permeabilized HEK293 cells in the presence of 10 μM ionomycin. n = 11. **I.** Intensity from **H** was normalized and fitted with the 1:1 binding equation to get an *in situ* Ca^{2+} K_d of 3.23 ± 1.38 mM. **J**. 0.1% DMSO control experiments in C2C12 cells. Scale bars, 20 μm.

A

Presynaptic

VDCC

ΔV

CaSR

IP$_3$

PMCA

Mito

$[Ca^{2+}]_i = $ 50-100 nM

mGluR1/5

Postsynaptic

ER

MCU

ER

$[Ca^{2+}]_{ER} = $ 1.0 mM

SERCA 0.05-5 s

AMPAR

$[Ca^{2+}]_c = ?$

IP$_3$R 10-60 s

$[Ca^{2+}]_{ER} = $ 1.0 mM

nAchR

RyR 1-5 ms

Action potential 1-5 ms

NMDAR

$[Ca^{2+}]_i = $ 50-100 nM

$[Ca^{2+}]_o = $ 1.1-1.8 mM

NCX

Calcium

TRP

Neurotransmitters

B

C

Ionomycin + Ca^{2+}

Soma
Primary Branchpoints
Primary Dendrites
Secondary Branchpoints
Secondary Dendrites

$\Delta F/F_0$

Time (sec)

D

■ Soma
■ Primary Branchpoints
■ Primary Dendrites
■ Secondary Branchpoints
■ Secondary Dendrites

$\Delta F/F_0$

E

Basal $[Ca^{2+}]_{ER}$ (µM)

*
*

Soma
Primary branchpoints
Primary dendrites
Secondary branchpoints
Secondary dendrites

Supplemental Figure 4. Neuron Ca^{2+} signaling and G-CatchER$^+$ response in mouse hippocampal neurons, related to Figure 3.
A. Schematic of Ca^{2+} sources and estimated concentrations at a typical excitatory chemical synapse. **B**. Example of a primary hippocampal neuron cultured 13 days *in vitro* transfected with G-CatchER$^+$. **C&D**. Traces and amplitude of G-CatchER$^+$ in response to 50 µM ionomycin and 10 mM Ca^{2+} in hippocampal neurons. **E.** Estimated absolute ER Ca^{2+} concentration in different neuronal regions using G-CatchER$^+$. Scale bar is 20 µm. Error bars are ± SEM, One-way ANOVA, Tukey's multiple comparisons.
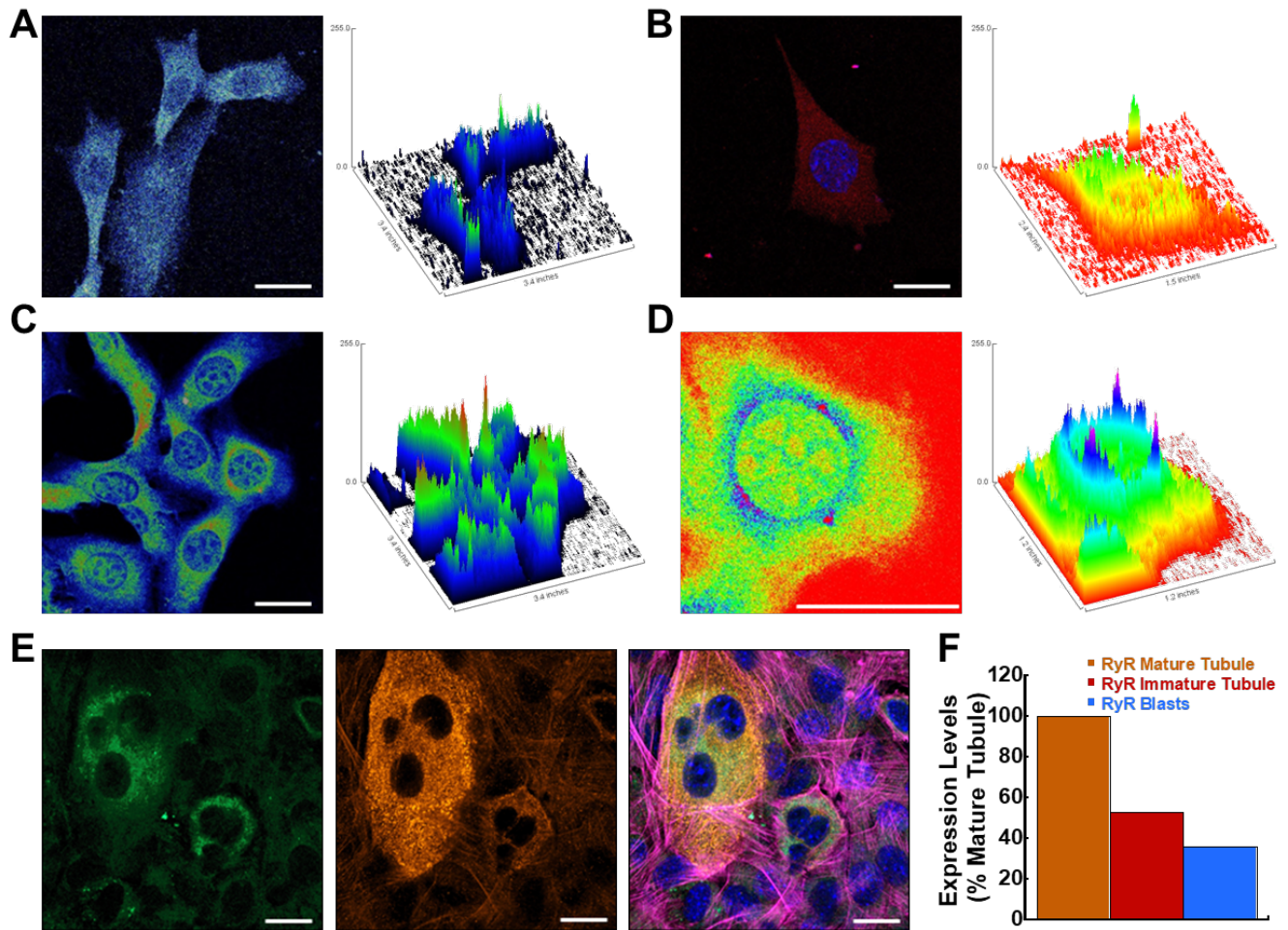
Supplemental Figure 5. Differential cellular distribution of RyR and SERCA in C2C12 cells, related to Figure 4 and Figure 5.
A&C. Confocal image of RyR **(A)** or SERCA1/SERCA2 **(C)** under rainbow RGB colors where red is high signal and blue is the low signal. *Right,* surface plot of these cells. **B&D.** A single C2C12 cell under spectrum colors where purple is the high signal and red is the low signal for RyR **(B)** or SERCA1/SERCA2 **(D)**. *Right,* surface plot of the cell. **E.** G-CatchER$^+$ (green), RyR (orange), Phalloidin (magenta) and DAPI (blue) in C2C12 cells. **F.** RyR expression for blasts (single nuclei), immature tubule (2-3 indistinct nuclei), and mature tubule (≥ 3 distinct nuclei). 1.9 fold more RyR is found in mature tubule over forming tubule and 2.8 fold more in tubule versus blast cells. Scale bars are 20 μm.
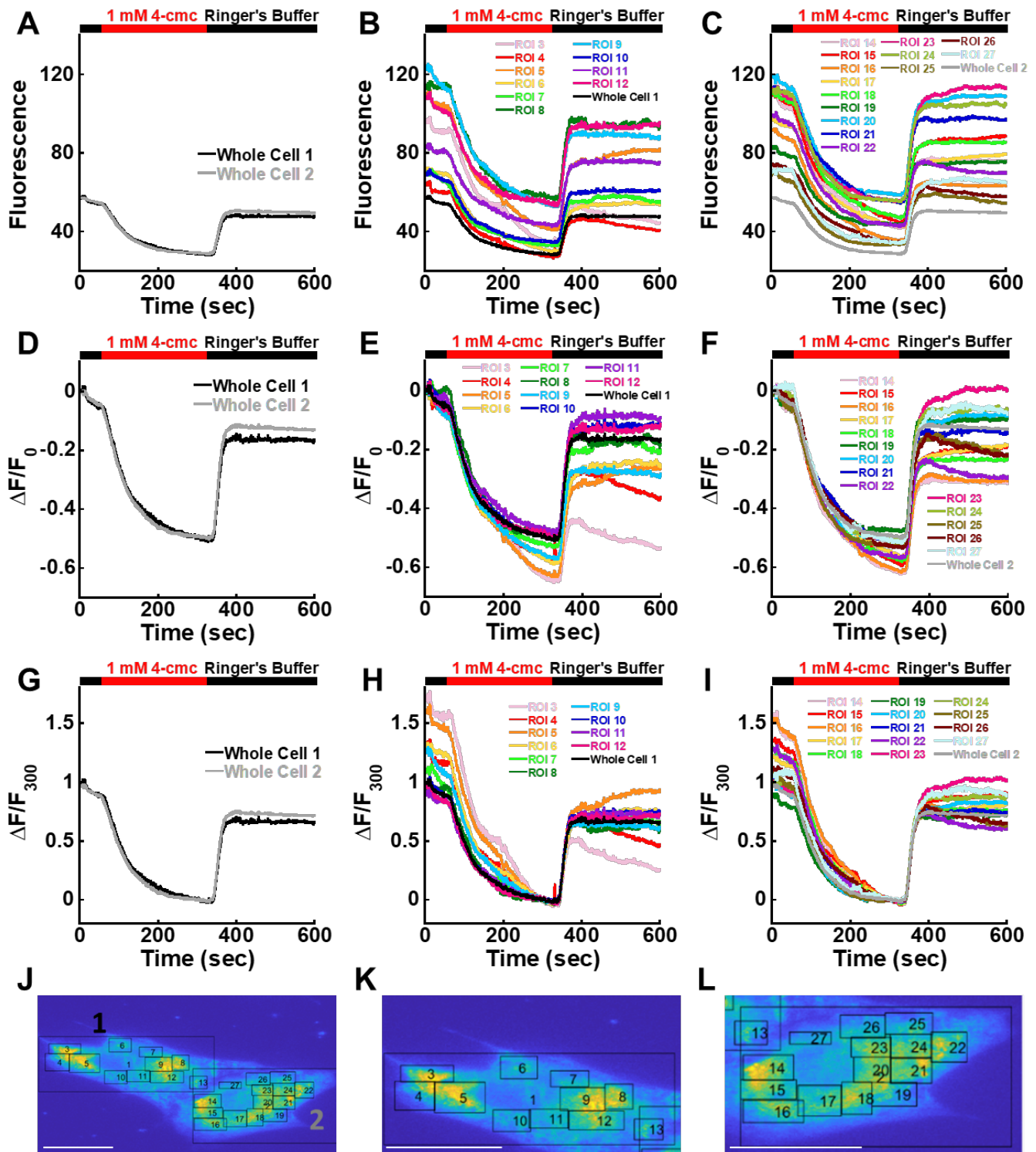
Supplemental Figure 6. G-CatchER⁺ monitors regional differential responses, related to Figure 4.

A-I. C2C12 cells transfected with G-CatchER⁺ and treated with 1 mM 4-cmc. The cells were examined as raw unprocessed data (**A-C**), normalized to starting as $(F-F_0)/F_0$ (**D-F**), and normalized to release as $(F-F_{300})/F_{300}$ (**G-I**). There is a large variance in response between the ROIs compared to the whole cell analysis, especially on the recovery phase. **J.** The whole cells where cell 1 is black and cell 2 is gray for plots A, D, and G. K. ROIs by number 3-12 on cell 1 from J as plotted in B, E, and H. L. ROIs by number 14-27 on cell 2 from J as plotted in C, F, and I. Scale bars are 20 μm.

A. Basal [Ca²⁺]ER (µM) — C2C12, Cos-7, HEK293, HeLa

B. 1 mM / 0.5 mM 4-cmc — Δ[Ca²⁺]ER (µM) — C2C12, Cos-7, HEK293, HeLa

C. 50 µM CPA — Δ[Ca²⁺]ER (µM) — C2C12, Cos-7, HEK293

D. 500 µM ATP — Δ[Ca²⁺]ER (µM) — C2C12, Cos-7, HEK293

E. 100 µM Histamine — Δ[Ca²⁺]ER (µM) — HeLa

F.

Cell Type	Drug Type	HILO Imaging		
		[Drug] (µM)	Absolute Δ[Ca²⁺] (µM)	Cell #	BR

Cell Type	Drug Type	[Drug] (µM)	Absolute Δ[Ca²⁺] (µM)	Cell #	BR
C2C12	4-cmc	1000	714.6 ± 47.6	10	3
Cos-7	4-cmc	500	362.3 ± 65.8	14	3
HEK293	4-cmc	500	306.9 ± 25.4	16	3
HeLa	4-cmc	1000	674.0 ± 36.4	20	3
C2C12	CPA	50	282.9 ± 32.4	12	3
Cos-7	CPA	50	242.5 ± 31.5	15	3
HEK293	CPA	50	392.6 ± 36.8	23	3
C2C12	ATP	500	187.5 ± 25.0	14	3
Cos-7	ATP	500	101.9 ± 17.6	11	3
HEK293	ATP	500	272.3 ± 25.0	19	3
HeLa	Histamine	100	351.6 ± 36.3	16	3

Supplemental Figure 7. Quantitative measurement of G-CatchER⁺ in different cell lines following addition of stimulatory or inhibitory agents, related to Table 1.
A. Basal ER Ca²⁺ estimation using G-CatchER⁺ in different cell lines. **B-F.** Estimated absolute ER Ca²⁺ change in response to 4-cmc, CPA, ATP and histamine in different cell lines using G-CatchER⁺.

Supplementary Table 1. Determined and reported Kd values for G-CatchER⁺ and other sensors, related to Figure 1.

Sensor Variant	λ_{ex} (nm)	0 mM KCl Buffer		KCl Buffer		Other Buffer	
		K_d (mM)	F_{max}/F_{min}	K_d (mM)	F_{max}/F_{min}	K_d (mM)	F_{max}/F_{min}
CatchER	488	0.2 ± 0.1	1.6 ± 0.1	0.9 ± 0.2	1.1 ± 0.2	-----	-----
G-CatchER-X	488	0.3 ± 0.1	2.1 ± 0.1	1.7 ± 0.1	1.3 ± 0.1	-----	-----
G-CatchER-XY	488	2.0 ± 0.6	1.5 ± 0.1	0.8 ± 0.1	1.2 ± 0.1	-----	-----
G-CatchER-XZ	488	1.0 ± 0.2	1.5 ± 0.1	5.1 ± 1.2	1.1 ± 0.1	-----	-----
G-CatchER⁺	488	1.2 ± 0.2	1.6 ± 0.1	-----	-----	-----	-----
D1ER	436 (CFP)	-----	-----	-----	-----	0.08	-----
	500 (YFP)	-----	-----	-----	-----	60	-----
G-CEPIA1er	499 (-Ca²⁺)	-----	-----	0.67 ± 0.02	4.7 ± 0.3	-----	-----
GCamP6-150	485	-----	-----	0.15	45.0	-----	-----

Zero KCl and KCl buffers are 10 mM Tris pH 7.4 with or without 150 mM KCl. Data represents mean ± SD. Kd – dissociation constant, λex – excitation wavelength, Fmax/Fmin – dynamic range in response to Ca2+ calculated using the fluorescence at maximal saturation divided by the fluorescence with no Ca2+ present. Data collected at room temperature. Samples prepared in 10 mM Tris pH 7.4 with or without 150 mM KCl. Fluorescence slit widths were 0.25 mm for excitation and emission. Dashed lines indicate data not available. G-CatchER-X is S175G mutation, G-CatchER-XY is S175G and Y39N mutation, G-CatchER-XZ is S175G and S30R mutation, and G-CatchER+ is S175G, Y39N and S30R mutations. All CatchER variants were done in 0 mM KCl buffer and 150 mM KCl buffer. GCamP6-150 was done in 100 mM KCl and 50 mM MOPS buffer. G-CEPIA1er was done in KCl MOPS buffer. D1ER done in undisclosed buffer8,35.

Supplementary Table 2. Ca^{2+} effect on the optical properties of G-CatchER^{+} and other CatchER variants *in vitro*, related to Figure 1.

Variant	$^{a}\phi$		$^{b}\varepsilon$ (mM^{-1}cm^{-1})		^{c}Brightness (mM^{-1}cm^{-1})	
	0 mM Ca^{2+}	5 mM Ca^{2+}	0 mM Ca^{2+}	5 mM Ca^{2+}	0 mM Ca^{2+}	5 mM Ca^{2+}
CatchER	0.78 ± 0.01	0.57 ± 0.01	7.50 ± 0.01	14.88 ± 0.15	5.47 ± 0.03	8.48 ± 0.01
G-CatchER-X	0.80 ± 0.01	0.83 ± 0.03	11.00 ± 0.05	14.14 ± 0.01	8.74 ± 0.13	11.81 ± 0.36
G-CatchER^{+}	0.70 ± 0.01	0.64 ± 0.01	10.52 ± 0.16	15.15 ± 0.04	7.27 ± 0.18	9.72 ± 0.05
149E	0.59 ± 0.01	0.51 ± 0.01	25.40 ± 0.06	40.00 ± 0.09	14.91 ± 0.07	20.40 ± 0.10
149E Y39N	0.59 ± 0.01	0.52 ± 0.01	22.68 ± 0.07	37.30 ± 0.12	13.34 ± 0.12	19.46 ± 0.18
149E S30R	0.68 ± 0.01	0.58 ± 0.01	17.61 ± 0.16	34.66 ± 0.09	11.96 ± 0.12	20.28 ± 0.11

Data presented is mean ± SD. Samples prepared in 10 mM Tris pH 7.4 with 10 µM EGTA. Experiments conducted at room temperature. Fluorescence excited at 488 nm and fluorescence excitation and emission slit widths were 0.1 mm and 0.6 mm, respectively. EGFP quantum yield was measured as 0.6 and used as the reference in the calculation. The 44 mM^{-1}cm^{-1} extinction coefficient at 447 nm absorbance peak for all FPs was used to calculate the extinction coefficient of the variants.

$^{a}\phi$ quantum yield is the ratio of photons emitted to photons absorbed.

$^{b}\varepsilon$ extinction coefficient is how strongly a compound absorbs light at a given wavelength.

^{c}Brightness is the perceived intensity of color. ϕ x ε

Supplementary Table 3. Chromophore pK$_a$ of G-CatchER$^+$ and other CatchER variants, related to Figure 1.

Variant	^{a}pK$_a$	
	0 mM Ca^{2+}	**5 mM Ca^{2+}**
^{b}**CatchER**	7.59 ± 0.03	6.91 ± 0.03
G-CatchER-X	7.71 ± 0.01	6.78 ± 0.00
G-CatchER$^+$	7.37 ± 0.01	6.80 ± 0.01
149E	6.47 ± 0.02	6.44 ± 0.01

Data presented is mean ± SD from fluorescence intensities were excited at 488 nm. Experiment done at room temperature. pH values were recorded before and after data collection. Final values were used for curve fitting.
^{a}pK$_a$ is the negative log of the acid dissociation constant which reflects the protonation state of the variant chromophore.
^{b}Reported values of CatchER are from the cited reference.

Transparent Methods

Chemicals and Reagents

The *E. coli.* strain DH5α, the plasmid vector pCDNA3.1(+), was purchased from Invitrogen. All the restriction enzymes, T4 DNA ligase, and T4 polynucleotide kinase (PNK) were purchased from New England Biolabs. DNA sequencing for all clones was carried out by GENEWIZ Inc. Plasmid extraction was carried out using the QIAGEN mini-prep and maxi-prep kits. C2C12, Cos-7, HEK-293 and HeLa cells were purchased from American Type Culture Collection (ATCC). (S)-3,5-DHPG (10 mM stock in buffer) and thapsigargin (1 mM stock in DMSO) were from Tocris. 4-cmc (100 mM stock in buffer), CPA (50 mM stock in DMSO), histamine (100 mM stock in buffer) and ATP (100 mM stock in buffer) were from Sigma-Aldrich. ER-Tracker Red, Alexa Fluor™ 633 Phalloidin and ProLong gold antifade mountant with DAPI were from Invitrogen. Mouse anti-ryanodine receptor antibody [34C], rabbit anti-ryanodine receptor antibody [EPR21796], mouse anti-SERCA1 ATPase antibody [VE121G9] and mouse anti-SERCA2 ATPase antibody [2A7-A1] were from abcam. pCMV-G-CEPIA1er was a gift from Dr. Yubin Zhou at Texas A&M University.

Cloning of G-CatchER⁺

CatchER was designed as previously detailed(Tang et al., 2011). To create G-CatchER⁺ containing the S175G, S30R, and Y39N mutations, point mutations were incorporated sequentially into CatchER in both vectors using 5'-AAGTTCAGCGTGCGCGGCGAGGGCGAG-3' and 5'-CTCGCCCTCGGCGCGCACGCTGAACTT-3' for S30R, 5'-GGCGATGCCACCAACGGCAAGCTG-3' and 5'-CAGCTTGCCGTTGGTGGCATCGCC-3' for Y39N, and 5'-GAGGACGGCGGCGTGCAGCT-3' and 5'-AGCTGCACGCCGCCGTCCTC-3' for S175G. G-CatchER⁺ was cloned into the pcDNA3.1+ vector using BamH1 and EcoR1 restriction enzyme sites. pDsRed2-JP45 was kindly provided by Dr. Francesco Zorzato. To create the G-CatchER⁺-JP45 fusion construct, dsRed was replaced with CatchER using BamH1 and Not1 restriction sites. Proper insertion of CatchER at the C-terminus of JP45 was confirmed by DNA sequencing using the forward primer 5'-GAGAAGCCAAGTAAAGGGGAGAAACTGAAG-

3' representing a small sequence of DNA at the C-terminus of JP45. The S175G, S30R, and Y39N mutations were then added to the CatchER-JP45 construct to make G-CatchER$^+$-JP45.

Expression and purification of G-CatchER$^+$ and variants

The GECI CatchER was created to monitor Ca^{2+} transients in the ER/SR and measure Ca^{2+} concentration in said organelles through a novel mechanism where the binding of Ca^{2+} on the surface of the protein induces an increase in fluorescence intensity. Because of improper formation of chromophore of CatchER at 37°C in mammalian cells (Tang et al., 2011), the probe was optimized to improve the fluorescence at 37°C resulting in the G-CatchER$^+$ series of variants. To obtain large amounts of the probes for *in vitro* analysis, the sensors were expressed and purified with high yield as previously detailed (Zhang et al., 2013). Briefly, pET28a vectors containing variant DNA were transformed into BL21(DE3) gold cells. Variants were expressed at 25°C following the addition of 0.2 mM IPTG in Luria Bertani (LB) media with 30 mg/mL of kanamycin. After centrifugation, cell pellets were re-suspended in 20-30 mL of lysis buffer (20 mM Tris, 100 mM NaCl, 0.1% Triton X-100, pH 8.0) and sonicated. The resulting lysate containing the protein of interest was centrifuged, and the supernatant was filtered and applied to a 5 mL Ni^{2+}-NTA HiTrap^{TM} HP chelating column (GE Healthcare) for HisTag purification using an imidazole gradient. To ensure protein purity and complete removal of imidazole, pure protein fractions were concentrated to 1 mL and buffer exchanged on a Superdex 200 gel filtration column (GE Healthcare) using 10 mM Tris pH 7.4 at 1 mL/min. Samples were taken during the expression and purification processes for SDS-PAGE analysis.

To determine if the mutations did improve the thermostability and brightness of the sensor at 37°C, each variant, including CatchER, was expressed in C2C12 myoblast cells at 37°C and imaged using a Leica DM6000 fluorescence microscope using previously established protocols (Reddish et al., 2017). C2C12 cells were seeded at a density of 40% and transfected on 22 mm x 40 mm glass microscope slides (Fisherbrand®) in 6 cm dishes. Images were taken from 8 fields of view on each slide. The intensity of the cells from each area was quantified using Image J and plotted with error using K-graph.

in vitro K_d of G-CatchER$^+$ and variants using fluorescence spectroscopy

Fluorescence measurements of G-CatchER$^+$ with increasing Ca^{2+} concentrations were done in order to obtain the affinity of the sensor for Ca^{2+} *in vitro*. Samples of 10 μM sensor with 5 μM ethylene glycol tetra acetic acid (EGTA) were prepared in triplicate in 1 mL volumes in 10 mM Tris, pH 7.4. The samples were placed in quartz fluorescence cuvettes, and metal ion was titrated into each sample, in a step wise manner, using 0.1 M and 1 M metal stock solutions. The fluorescence response of the sensor to increasing Ca^{2+} concentrations was monitored using a fluorescence spectrophotometer (Photon Technology International, Canada) with the *Felix32* fluorescence analysis software. Slit widths were set at 0.25 or 0.3 mm for excitation and emission. The samples were excited at 395 nm and 488 nm with emission collected from 410-600 nm for 395 nm excitation and from 500-600 nm for 488 nm excitation. The absorbance spectra before and after titration were obtained using a Shimadzu UV-1601 spectrophotometer. Fluorescence and absorbance traces were plotted using Kalidegraph (KGraph). The data was normalized to show the relative change in relation to the basal fluorescence using the following equation,

$$y = \frac{(F - F_{min})}{(F_{max} - F_{min})} \qquad \text{equation 1}$$

where F is the fluorescence intensity at any point, F_{min} is minimum fluorescence intensity, and F_{max} is the maximum fluorescence intensity. The normalized data was then plotted and fitted in KGraph to obtain the dissociation constant (K_d) using the following equation for 1:1 binding,

$$\frac{[PM]}{[P_T]} = \frac{[M_T]}{K_d + [M_T]} \qquad \text{equation 2}$$

where [PM] is the concentration of protein-metal complex, [P$_T$] is the total protein concentration, [M$_T$] is the total metal concentration, and K_d is the dissociation constant. [PM]/[P$_T$] represents the change in complex formation. A complete derivation of the 1:1 binding equation was done in previous work(Zhang et al., 2013). To determine the Ca^{2+} K_d at physiological concentrations of salt, Tris buffer and KCl were dissolved in H$_2$O to make the final concentrations of each 10 mM and 150 mM, respectively, and the pH was adjusted to 7.4. Subsequent titrations proceeded as previously stated.

Stop flow kinetics for G-CatchER⁺

 The kinetics of G-CatchER⁺ and G-CEPIA1er were determined using a SF-61 stopped flow spectrofluorometer (10-mm path length, 2.2 ms dead time at room temperature; Hi-Tech Scientific) at room temperature. For G-CatchER⁺, fluorescence intensity changes were recorded with a 510/30 nm band pass filter with excitation at 488 nm; whereas, for G-CEPIA1er, a 530 nm long pass filter with excitation at 498 nm was used. For association kinetics, G-CatchER+ and G-CEPIA1er in 0 Ca^{2+} buffer were mixed with the same buffer containing increasing concentration of Ca^{2+}. For disassociation kinetics, G-CatchER⁺ and G-CEPIA1er were examined in a buffer with concentration of Ca^{2+} around K_d and were mixed with 5 mM EGTA. The raw data was fitted using either monoexponential (equation 3) or biexponential (equation 4) equations.

$$F = A1 \times \exp(R1 \times t) + C \qquad\qquad\qquad \text{equation 3}$$

$$F = A1 \times \exp(-R1 \times t) + A2 \times \exp(-R2 \times t) + C \qquad \text{equation 4}$$

A1 and A2, the amplitude of the fluorescence change at the first phase and second phase; R1 and R2, the observed rate constant at the first phase and second phase; and t, the time.

Fluorescence lifetime measurements

G-CatchER⁺ in H_2O was exchanged by D_2O (95% D) and the final pH and pD were adjusted to 7.4 and 7.8, respectively. For neutral and anionic forms of G-CatchER⁺, a 372 nm laser was used to excite G-CatchER⁺ and emission at 440 nm and 510 nm were detected, accordingly. 1024 data points were collected for the neutral form of G-CatchER⁺ in 5 ns, however, for the anionic form, 1024 data points were collected in 20 ns. All measurements were carried out at 25ºC. The time course of fluorescence decay was deconvoluted by the program FFIT developed and fitted using an exponential equation (Bayley et al., 1984).

Cell culture and transfection of G-CatchER$^+$ and G-CatchER$^+$-JP45

Cell culture and transfection of G-CatchER$^+$ and G-CatchER$^+$-JP45 was done and modified based on established protocols (Reddish et al., 2017). We chose HEK293 and Cos-7 cells for their high transfection ability, their accessibility, and their rapid growth. Cos-7 cells have a greater cytosol to nuclear ratio and are also very flat which, improves focusing during image acquisition. C2C12 myoblast cells were chosen because they are non-differentiated skeletal muscle cells that can differentiate into myotubes which could be used to compare differences in calcium transients between immature and maturing cells. These cells were maintained in Corning™ Dulbecco's modified Eagle's medium (DMEM) with L-Glutamine, 4.5g/L supplemented with 10% fetal bovine serum (FBS) and high glucose (4.5 g/L) at 37°C. G-CatchER$^+$ was transfected into cells using Lipofectamine 3000 (Life Technologies) by following the manufacturer's instructions. HEK293, Cos-7 or HeLa cells were seeded onto sterilized 22 mm x 40 mm glass microscope slides in 6 cm dishes. The next day, cells were transfected with G-CatchER$^+$ or G-CatchER$^+$-JP45 cDNA and incubated for 4-6 h at 37°C. After incubation, cells were washed with 5-6 mL of HBSS and replaced with 3 mL of fresh DMEM and incubated for 48 h at 37°C to allow expression of G-CatchER$^+$ and G-CatchER$^+$-JP45. For C2C12 myoblast cells, transfection material was incubated for 24 h at 37°C and then removed and imaged as stated above. For myotube imaging and staining, slides were pretreated with laminin to allow high confluency cell growth. The first transfection for myotubules was done as stated above for C2C12 cells using G-CatchER$^+$ or G-CatchER$^+$-JP45 on day 0, then on day 2 the transfection was repeated, and again on day 4 the transfection was repeated where imaging was done on days 6-8. Washing with fresh DMEM was done after each transfection.

Primary hippocampal neuron cultures were generated from postnatal day 0-1 mice as previously described (Wall et al., 2018). Neurons were maintained in neuronal feeding media (Neurobasal media, ThermoFisher Scientific) containing 1% GlutaMAX (ThermoFisher Scientific), 2% B-27 (ThermoFisher Scientific), 4.8 µg/mL 5-Fluoro-2'-deoxyuridine (Sigma), and 0.0002 mg/mL Gentamicin (Sigma) and fed every 3-4 days via half neuronal feeding media exchange. At 11-12 days *in vitro* cells were transfected with G-CatchER$^+$ DNA and mCherry (used as a cell fill) DNA using Lipofectamine 2000 Reagent (ThermoFisher Scientific) using a modified protocol (Mabb et al., 2014).

The electroporation procedure was as described previously (DiFranco et al., 2009). Briefly, 8- to 14-week-old mice were anaesthetized using isofluorane, and 7.5 µl of 2 mg/ml Hyaluronidase in RNase-free Tyroide's Buffer (Sigma-Aldrich, #H3506) was injected under the footpad. The mice were left 1 h under supervision, and subsequently, the pcDNA$^+$3.1 plasmids carrying G-CatchER$^+$ and G-CatchER$^+$-JP45 were injected into the footpad. Ten minutes post-injection, FDBs were electroporated using acupuncture needles placed parallel and perpendicular to the long axis of the foot (with 1 cm distance), and twenty pulses (100v/cm, 20 ms duration and 1 Hz of frequency) were given. Six to ten days post–transfection, the mice were sacrificed and FDBs were isolated by enzymatic dissociation at 37°C for 60 min in Krebs Ringer solution without Ca^{2+} (pH 7.4), containing 0.2% collagenase I (Sigma-Aldrich, C-0130). Enzymatic digestion was terminated by washing the muscle with Tyrode's solution (pH 7.4) and single fibers were isolated.

Confocal imaging of G-CatchER$^+$ and G-CatchER$^+$-JP45

We used confocal laser scanning microscopy (CLSM) Zeiss LSM800 on fixed cells. These cells were stained with either BODIPY ER-Tracker Red (Invitrogen) per their protocol at 1 µM for staining the ER, Alexa Fluor™ 633 Phalloidin (Invitrogen) per their protocol for staining actin, anti-ryanodine receptor antibody [34C] (abcam), anti-ryanodine receptor antibody [EPR21796] (abcam), anti-SERCA1 ATPase antibody [VE121G9] (abcam), anti-SERCA2 ATPase antibody [2A7-A1] (abcam), and all with ProLong gold antifade mountant with DAPI (Invitrogen) for staining the nucleus. G-CatchER$^+$ or G-CatchER$^+$-JP45 were transfected into the cells two days before fixing for blast cells and were triple transfected over one week for myotubules. Cells were fixed with 3.7% Thermo Scientific™ Pierce™ 16% Formaldehyde (w/v), Methanol-free, permeabilized with 0.1% Triton X-100, and non-specific binding was blocked with 1-5% Bovine Serum Albumin (BSA) all in phosphate buffered saline (PBS).

As for confocal imaging of G-CatchER$^+$ or G-CatchER$^+$-JP45 in C2C12 myoblasts and myotubes, G-CatchER$^+$ or G-CatchER$^+$-JP45 were transfected into the cells two days before fixation. The distribution of G-CatchER$^+$ is more widespread than G-CatchER$^+$-JP45 which is more concentrated near certain sections of the cell than other,

presumably the longitudinal SR. Both sensors overlay well with ER-Tracker Red, showing that although their specific ER locations may differ they still are both situated solely in the ER. HILO microscopy more thoroughly shows the network type pattern of the ER in the cells expressing G-CatchER⁺.

Epifluorescence imaging of G-CatchER⁺

G-CatchER⁺ was transiently transfected into cells grown on coverslips and cultured for 48 h at 37°C. Cells were washed twice with 2 mL of physiological Ringer buffer (10 mM HEPES, 121 mM NaCl, 2.4 mM K_2HPO_4, 0.4 mM KH_2PO_4, 1.2 mM $MgCl_2$, 1.8 mM $CaCl_2$ at pH 7.4). The coverslips are mounted on a bath chamber and placed on the stage of a fluorescence microscope. The cells were illuminated with 488 nm and the fluorescence at an emission wavelength 510 nm was recorded in real time as the concentration of ER/SR Ca^{2+} was perturbed with 4-cmc, CPA, or ATP. All experiments were performed at room temperature on a Leica DM6100B inverted microscope with a Hamamatsu cooled EM-CCD camera and illuminated with a Till Polychrome V Xenon lamp.

HILO imaging of G-CatchER⁺ and G-CatchER⁺-JP45

HILO microscopy was accomplished using a Nikon TiE inverted microscope with Andor Ixon Ultra 888 EMCCD Camera. Briefly, a fiber coupled 488 nm laser (Oxxius) was collimated and introduced into the optical train of the microscope. The laser was then focused at the back focal plane of a 100X TIRF objective (N.A. 1.49, Nikon) by using an achromatic optical lens (Thorlabs) with 200 mm focal length. The laser collimation system and focusing lens were both mounted on a mechanic translation stage (Thorlabs) so that its optical axis of incident laser could be laterally shifted to change the incident angle of laser at the cell-coverslip interface. The HILO imaging condition was achieved by operating at sub-critical angles of the total internal reflection. Since the thickness of cells as well as the depth of ER structure varies among individual cells, the best HILO imaging conditions were achieved by carefully tuning the incident angle of the excitation laser. Moreover, the epifluorescence images used for comparing with HILO imaging was taken by setting the incident angle at 0 degrees. Large scale data

analysis of live cell imaging of G-CatchER$^+$ and G-CatchER$^+$-JP45 using HILO imaging was done with self-written MATLAB script.

Correlation between G-CatchER$^+$ and ER proteins

C2C12 cells were cultured in Ibidi flow chamber μ-Slide I Luer 0.8 mm and transfected using Lipofectamine 3000 at 2 μg/mL of G-CatchER$^+$ DNA. Imaging of the flow chamber was done using HILO imaging microscope as described above. In live cell experiments, the 4-cmc drug was introduced into the flow chamber by using a syringe pump at a flow rate of 1 mL/min. Then we mark the area on the outside of the chamber using marker and draw next to the imaged cell on bright field. The cells were immediately fixed after live cell imaging experiments with 3.7% Thermo Scientific™ Pierce™ 16% formaldehyde (w/v), methanol-free in PBS for 15 mins at room temperature. Cells were washed with 0.1% Triton X-100 in PBS, and non-specific binding was blocked with 5% BSA in PBS for 1 hour. The samples were incubated in 1% BSA with 1:500 of anti-GFP antibody (abcam), 1:100 of anti-ryanodine receptor antibody [EPR21796] (abcam), and 1:250 of both anti-SERCA1 ATPase antibody [VE121G9] (abcam) and anti-SERCA2 ATPase antibody [2A7-A1] (abcam) overnight at 4°C. Cells were aspirated and washed three times with PBS at room temperature then incubated at 1:500 with goat anti-chicken Alexa Fluor 488 (abcam) and 1:250 with both goat anti-mouse Alexa Fluor 555 (abcam) and goat anti-rabbit Alexa Fluor 633 (Thermofisher). After rinsing 3 times (10 min each time) in PBS the slides were mounted with Invitrogen™ ProLong™ Gold Antifade Mountant with DAPI for staining the nucleus. We used confocal laser scanning microscopy (CLSM) Zeiss LSM800 on fixed cells and Airyscan technology. Correlation analysis between G-CatchER$^+$ signal and ER proteins (RyR, SERCA) was analyzed using self-written MATLAB script.

Neuron imaging

For live imaging of G-CatchER$^+$ in neuron cultures, G-CatchER$^+$-transfected neurons were transferred to artificial cerebrospinal fluid (ACSF; 124 mM NaCl, 3 mM KCl, 2 mM CaCl$_2$, 2 mM MgCl$_2$, 10 mM HEPES, 10 mM D-Glucose, pH 7.4) pre-warmed to 37°C. Neurons were imaged using HILO microscopy at 2 frames per second

with the protocol and equipment discussed above. Once a G-CatchER$^+$ transfected neuron was identified, it was inspected using the mCherry cell fill for healthy cell morphology. G-CatchER$^+$ signal was acquired at baseline, whereupon a drug treatment was gently washed in (1 mM 4-cmc, 50 μM CPA, or 100 μM DHPG all in ACSF pre-warmed to 37°C) with a syringe connected to tubing that extended into the imaging chamber. Following imaging under treatment conditions, drugs were washed out with ACSF pre-warmed to 37°C. Maximum fluorescence (Fmax) of G-CatchER$^+$ was obtained by applying 50 μM ionomycin and 10 mM Ca^{2+}. Basal [Ca^{2+}]$_{ER}$ in different neuronal regions was calculated using an established method (de Juan-Sanz et al., 2017).

Drosophila strains and husbandry

All flies were maintained on standard cornmeal-molasses-agar media. All genetic crosses were raised at 29°C in 12:12 light:dark cycle. The following *Drosophila* stocks used in this study were obtained from the Bloomington *Drosophila* Stock Center: Mef2^{GAL4}: *y[1] w[*]; P{w[+mC]=GAL4-Mef2.R}3* (BDSC# 27390); UAS-GFP: *w[1118]; P{y[+t7.7] w[+mC]=10XUAS-IVS-mCD8::GFP}su(Hw)attP1* (BDSC# 32187); UAS-Sec61β::tdTomato: *w[1118]; P{y[+7.7] w[+mC]=20XUAS-tdTomato-Sec61beta}attP2* (BDSC# 64747), and the background genetic control strain: *w[1118]* (BDSC# 3605).

Molecular cloning and *Drosophila* transgenic production

We utilized Gateway cloning technology for generating the *UAS-G-CatchER$^+$* plasmid. We performed cloning based on the Invitrogen protocol for MultiSite Gateway Pro Plus (Vector module (ref: 45-2100), BP Clonase (ref: 11789-020) and LR Clonase (ref: 12538-120)). We inserted G-CatchER$^+$ into the donor vector by performing a BP reaction with G-CatchER$^+$ in the pcDNA3.1 plasmid backbone and pDONR^{tm} 221 P5-P2. Next, we combined pENTR L1-20XUAS-R5 (Addgene# 32302) and pDONR^{tm} 221 P5-G-CatchER+-P2 (BP reaction product, this study) into the *Drosophila* destination vector pDESTsvaw (Addgene# 32318) by performing the LR reaction. *Drosophila* transgenic production was performed by GenetiVision Corporation (Houston, TX). PhiC31 integrase technology was used to insert *UAS-G-CatchER$^+$* into the 2nd (VK1) and 3rd chromosome (VK20) *attP* landing sites.

in vivo* imaging of genetically-encoded G-CatchER⁺ in *Drosophila

In vivo confocal imaging of muscle morphology and SR localization of G-CatchER⁺ was performed as previously described (Turner et al., 2016, Patel and Cox, 2017). Briefly, we mount live, intact, 3rd instar *Drosophila* larvae on a microscope slide using 1:5 solution of diethyl ether and halocarbon oil. *Drosophila* larvae were imaged using a Zeiss LSM 780 laser scanning confocal microscope, where z-stacks imaged for muscle morphology were acquired using an Apochromat 20x lens and SR localization acquired using an Apochromat 40x objective lens.

Cold-evoked imaging of SR Ca^{2+} dynamics was performed as previously described (Turner et al., 2016, Patel and Cox, 2017). Intact, live, 3rd instar *Drosophila* larvae were mounted on microscope slide with water and coverslip, where the coverslip was secured by stage clips. A PE120 thermal stage and T95 system controller from Linkam Scientific Instruments were used for delivering temperature stimuli to *Drosophila* larvae. We used the following cold stimulation regimen: an initial 1 minute baseline recording at 25°C; ramp down to 10°C at a rate of 20°C/minute; hold at 10°C for 30 seconds; ramp up to 25°C at 20°C/minute to return to baseline, repeating this cold stimulus regimen two additional cycles for a total of three stimulations. G-CatchER⁺ responses were recorded in intact, live *Drosophila* 3rd instar larvae using a Zeiss LSM 780 confocal with Neofluar 10x objective lens at 5.08 frames per second, 512 x 512 pixel resolution. G-CatchER⁺ fluorescence was analyzed using Fiji (Schindelin et al., 2012) by creating a grid of 85 ROIs of 30 x 100 pixels. Percent $\Delta F/F_0$ for all animals and ROIs was calculated using a custom R script and the following equation: $\Delta F / F_0 = \frac{F_{n\,frame} - average\,F_{frames\,1-300}}{average\,F_{frames\,1-300}}$

***Drosophila* larval locomotion assay**

Larval locomotion assay was performed using 3rd instar *Drosophila* larvae. Larvae were placed on 2% agarose gel and allowed to acclimate for 5 minutes at 25°C. To obtain high signal to noise ratio, we illuminated the agarose gel and larvae from below and imaged larvae from above using a Nikon D5300 DSLR camera at 30 frames per second. We recorded larval locomotion for 5 minutes. Raw larval locomotion videos were uncompressed using video to video convertor (videotovideo.org). The background was removed from original videos and exported as an image sequence via custom Fiji scripts. Larval locomotion was tracked using FimTrack (Risse et al., 2017). Larval locomotion consists of peristaltic linear forward motion with saccadic turns

and reverse locomotion. Additionally, the larvae may collide with a barrier or other larvae, which impairs locomotion tracking. Therefore, we analyzed only continuous 1-minute long locomotion tracks, where individual larvae did not collide with one another. FimTrack data of individual videos was compiled and processed using custom R scripts (Wickham et al., 2019; Bengtsson, 2018; R Core Team, 2017; R Studio Team, 2020). tSNE analyses were performed in R using a publicly available library for tSNE (Krijthe, 2015).

Statistics

Error bars indicate mean ± SEM. Student's t tests or One-way ANOVA were used to determine the significant difference.

Supplemental References

BAYLEY, P., AHLSTROM, P., MARTIN, S. R. & FORSEN, S. 1984. The Kinetics of Calcium-Binding to Calmodulin - Quin-2 and Ans Stopped-Flow Fluorescence Studies. *Biochemical and Biophysical Research Communications,* 120**,** 185-191.

BENGTSSON, H. 2018. matrixStats: Functions that apply to rows and columns of matrices and to vectors. R package version 0.54.0. https://CRAN.R-project.org/package=matrixStats.

DE JUAN-SANZ, J., HOLT, G. T., SCHREITER, E. R., DE JUAN, F., KIM, D. S. & RYAN, T. A. 2017. Axonal Endoplasmic Reticulum Ca(2+) Content Controls Release Probability in CNS Nerve Terminals. *Neuron,* 93**,** 867-881 e6.

DIFRANCO, M., QUINONEZ, M., CAPOTE, J. & VERGARA, J. 2009. DNA transfection of mammalian skeletal muscles using in vivo electroporation. J Vis Exp.

KRIJTHE, J.H. 2015. Rtsne: T-distributed stochastic neighbor embedding using a Barnes-Hut implementation. URL: https://github.com/jkrijthe/Rtsne.

MABB, A. M., JE, H. S., WALL, M. J., ROBINSON, C. G., LARSEN, R. S., QIANG, Y., CORREA, S. A. & EHLERS, M. D. 2014. Triad3A regulates synaptic strength by ubiquitination of Arc. Neuron, 82, 1299-316.

PATEL, A. A. & COX, D. N. 2017. Behavioral and Functional Assays for Investigating Mechanisms of Noxious Cold Detection and Multimodal Sensory Processing in Drosophila Larvae. *Bio Protoc,* 7.

R CORE TEAM. 2017. R: A language and environment for statistical computing. R Foundation for Statistical Computing, Vienna, Austria. https://www.R-project.org.

R STUDIO TEAM. 2020. RStudio: Integrated development for R. RStudio, PBC, Boston, MA. http://www.rstudio.com

REDDISH, F. N., MILLER, C. L., GORKHALI, R. & YANG, J. J. 2017. Monitoring ER/SR Calcium Release with the Targeted Ca2+ Sensor CatchER+. *JoVE (Journal of Visualized Experiments)***,** e55822.

RISSE, B., BERH, D., OTTO, N., KLAMBT, C. & JIANG, X. 2017. FIMTrack: An open source tracking and locomotion analysis software for small animals. *PLoS Comput Biol,* 13**,** e1005530.

SCHINDELIN, J., ARGANDA-CARRERAS, I., FRISE, E., KAYNIG, V., LONGAIR, M., PIETZSCH, T., PREIBISCH, S., RUEDEN, C., SAALFELD, S., SCHMID, B., TINEVEZ, J. Y., WHITE, D. J., HARTENSTEIN, V., ELICEIRI, K., TOMANCAK, P. & CARDONA, A. 2012. Fiji: an open-source platform for biological-image analysis. *Nat Methods,* 9**,** 676-82.

TANG, S., WONG, H. C., WANG, Z. M., HUANG, Y., ZOU, J., ZHUO, Y., PENNATI, A., GADDA, G., DELBONO, O. & YANG, J. J. 2011. Design and application of a class of sensors to monitor Ca(2+) dynamics in high Ca(2+) concentration cellular compartments. *Proceedings of the National Academy of Sciences of the United States of America,* 108**,** 16265-16270.

TURNER, H. N., ARMENGOL, K., PATEL, A. A., HIMMEL, N. J., SULLIVAN, L., IYER, S. C., BHATTACHARYA, S., IYER, E. P. R., LANDRY, C., GALKO, M. J. & COX, D. N. 2016. The TRP Channels Pkd2, NompC, and Trpm Act in Cold-Sensing Neurons to Mediate Unique Aversive Behaviors to Noxious Cold in Drosophila. *Curr Biol,* 26**,** 3116-3128.

WALL, M. J., COLLINS, D. R., CHERY, S. L., ALLEN, Z. D., PASTUZYN, E. D., GEORGE, A. J., NIKOLOVA, V. D., MOY, S. S., PHILPOT, B. D., SHEPHERD, J. D., MULLER, J., EHLERS, M. D., MABB, A. M. & CORREA, S. A. L. 2018. The Temporal Dynamics of Arc Expression Regulate Cognitive Flexibility. *Neuron,* 98**,** 1124-1132 e7.

WICKHAM, H., FRANCOIS, R., HENRY, L. & MÜLLER, K. 2019. dplyr: A grammar of data manipulation. R package version 0.8.0.1. https://CRAN.R-project.org/package=dplyr.

ZHANG, Y., REDDISH, F., TANG, S., ZHUO, Y., WANG, Y. F., YANG, J. J. & WEBER, I. T. 2013. Structural basis for a hand-like site in the calcium sensor CatchER with fast kinetics. *Acta Crystallographica Section D-Biological Crystallography,* 69**,** 2309-2319.